

Inverse Current in Coupled Transport: A Quantum Thermodynamic Framework for Energy and Spin-polarized Particle Currents

Shuvadip Ghosh,^{1,*} Nikhil Gupt,¹ and Arnab Ghosh¹

¹*Indian Institute of Technology Kanpur, Kanpur, Uttar Pradesh 208016, India*

The phenomenon of inverse current in coupled transport (ICC), where one induced current flows counter to two parallel thermodynamic forces, represents a strikingly counterintuitive behavior in transport processes [[Phys. Rev. Lett. 124, 11607 \(2020\)](#)]. Through an exactly solvable model of strongly coupled quantum dots, we provide a quantum thermodynamic framework to describe ICC in energy and spin-polarized particle currents, highlighting its potential applications for unconventional and autonomous nanoscale thermoelectric engines and refrigerators. Our analysis establishes a link between the microscopic and macroscopic descriptions of the entropy production rate, emphasizing the crucial role of thermodynamic forces and their conjugate fluxes in accurately characterizing genuine ICC. Here, the paradoxical behavior of ICC emerges from the symmetry breaking between particle and energy transitions, identified as the sufficient condition, while the attractive interaction between the coupled quantum dots is determined to be the necessary criterion for the ICC effect.

I. INTRODUCTION

Force and flux are two central thermodynamic quantities, interlinked through a cause-and-effect relationship. A thermodynamic force (\mathcal{F}) engenders a response in the form of a flux (J) within the system, causing a departure from equilibrium. For a single driving force, the resultant flux always aligns with the direction of the applied force, establishing a new equilibrium, consistent with the positive entropy production rate, $\dot{\Sigma} = J\mathcal{F}$ [1, 2]. This situation changes significantly in the presence of multiple force-flux pairs. For example, a thermal (energy) force \mathcal{F}_E and a particle force \mathcal{F}_N can drive both particle (J_N) and energy (J_E) currents. Consequently, the rate of entropy production near equilibrium is expressed as $\dot{\Sigma} = J_E\mathcal{F}_E + J_N\mathcal{F}_N$, where $J_E(J_N)$ is the thermodynamic flux conjugate to the thermodynamic force $\mathcal{F}_E(\mathcal{F}_N)$. This could lead to the possibility of Inverse Current in Coupled transport (ICC) when both forces are mutually parallel (i.e. $\mathcal{F}_E > 0$ and $\mathcal{F}_N > 0$), yet one of the induced currents flows *against* both forces (either $J_E < 0$ or $J_N < 0$). Although the sign of a current is a matter of convention, for ICC to occur, a current must flow simultaneously against both mutually parallel thermodynamic forces. Consequently, we set both $\mathcal{F}_E > 0$ and $\mathcal{F}_N > 0$ in $\dot{\Sigma} = J_E\mathcal{F}_E + J_N\mathcal{F}_N$, w.l.o.g, so that a negative current signals ICC [3]. An immediate consequence is that simultaneous ICC in both fluxes is impossible, as it would violate the second law of thermodynamics by yielding in a negative entropy production rate.

The ICC has only recently been demonstrated in classical Hamiltonian systems [3] and has been extended to Coulomb-coupled quantum dot (QD) systems [4, 5]. Although the phenomenon appears highly counterintuitive, it is not forbidden, as long as the overall entropy production rate remains positive. Though, recent attempts [4, 5] demonstrate ICC in quantum systems

with parallel-coupled Coulomb QDs, the simultaneous coupling of each thermal bath to both QDs makes it challenging to perform a systematic analysis in terms of proper thermodynamic forces and the corresponding fluxes. Moreover, Ref. [4, 5] treats gradients as thermodynamic forces, raising concerns when viewed in terms of proper thermodynamic forces.

To address this problem, we propose an exactly solvable model of three-terminal Coulomb-coupled QDs, an improvised variant of Sánchez-Büttiker model [6] which has been studied in the context of, such as quantum transport [7–10], quantum information [11–16] and thermoelectricity [17–28], thermal rectification [29–34], and others [35–39]. This model effectively reduces the problem of coupled transport with two mutually parallel forces and their corresponding fluxes, simplifying the overall analysis. The crux of our approach lies in identifying macroscopic and microscopic expressions of thermodynamic forces and fluxes, connected via total entropy production rate. Our findings highlight the critical role of QD interactions in establishing the ICC in energy and particle currents at near equilibrium. Most importantly, we derive the conditions for genuine ICC in both energy and (spin-polarized) particle currents, in compliance with the second law of thermodynamics.

The structure of the paper is as follows: Section II outlines our model, which is based on Coulomb-coupled QDs. We explore the system's dynamics in Sec. III, analyze steady-state currents in Sec. IV, and examine entropy production, including macroscopic and microscopic forces and fluxes, in Sec. V. Section VI provides a comparison between ICC and normal cross-effect and Sec. VII summarizes our results. Finally, we conclude in Sec. VIII.

II. MODEL

To investigate the ICC, it is essential to consider the coupled transport phenomenon, which involves energy and particle force-flux pairs. A Coulomb-coupled quan-

* shuvadipg21@iitk.ac.in

tum dot (QD) [6, 29, 31–34, 40] setup emerges as an ideal choice for this purpose. Our model consists of two quantum dots (QDs) that are strongly and capacitively coupled, labeled as the left (QD_L) and right (QD_R), as illustrated in [FIG. 1(a)]. The dots interact via a long-range Coulomb force, preventing particle exchange due to Coulomb blockade [29, 31, 34] while enabling energy exchange mediated by the Coulomb interaction (κ_c). Each QD could be tunnel-coupled to one or more reservoirs [6, 34, 40–44] allowing particle and energy exchange with leads. Since inter-dot particle hopping is restricted, generating particle current in the coupled QD setup requires at least one QD to be simultaneously coupled to more than one reservoir. On the other hand, our model ensures that no reservoir is connected to more than one QD to avoid unnecessary complexity. Clearly, both the above conditions cannot be met in a two-terminal setup. Therefore, a three-terminal model is absolutely necessary. Thus, w.l.o.g, we assume that QD_L is tunnel-coupled to two fermionic leads, labeled as a and b , located *above* and *below*, respectively [FIG. 1(a)]. In contrast, the other dot, QD_R , is tunnel-coupled to only a single reservoir on the right, labeled as r [FIG. 1(a)]. For spinless electrons, inter-dot interaction is always positive; however, we extend our study to spin-polarized [45–47] electrons. Consequently, we further assume that QD_L is coupled to spin-down (\downarrow) fermionic reservoirs i.e. a and b , and QD_R to spin-up (\uparrow) one (r). The Hamiltonian governing the coupled QD system is given by

$$H_S = \varepsilon_L \mathcal{N}_{L\downarrow} + \varepsilon_R \mathcal{N}_{R\uparrow} + \kappa_c \mathcal{N}_{L\downarrow} \mathcal{N}_{R\uparrow} + \kappa_s \sigma_{L\downarrow}^z \sigma_{R\uparrow}^z. \quad (1)$$

In Eq. (1), ε_α ($\alpha = L, R$), denotes the single-particle energy level of the α 'th QD. Due to the Coulomb blockade, the electron density in the dots is low, limiting the occupancy to either zero or one. The eigenstates of $QD_{L(R)}$ are $|0\rangle$ and $|\downarrow\rangle$ ($|\uparrow\rangle$), with energy eigenvalues 0 and ε_L (ε_R), respectively. The number operators are $\mathcal{N}_{L\downarrow} = d_{L\downarrow}^\dagger d_{L\downarrow}$ and $\mathcal{N}_{R\uparrow} = d_{R\uparrow}^\dagger d_{R\uparrow}$, where $d_{\alpha\sigma}^\dagger$ ($d_{\alpha\sigma}$) represent the electron creation and annihilation operators with spin $\sigma = \{\uparrow, \downarrow\}$, obeying $\{d_{\alpha\sigma}, d_{\alpha'\sigma'}^\dagger\} = \delta_{\alpha\alpha'} \delta_{\sigma\sigma'}$. The spin-spin interaction term [48] in Eq. (1) is expressed as $\sigma_{L\downarrow}^z = 1 - 2\mathcal{N}_{L\downarrow}$ and $\sigma_{R\uparrow}^z = 2\mathcal{N}_{R\uparrow} - 1$, where the spin operator σ^z satisfies the relations $\sigma_{L\downarrow}^z |\downarrow\rangle = -1 |\downarrow\rangle$ and $\sigma_{R\uparrow}^z |\uparrow\rangle = +1 |\uparrow\rangle$.

With strong capacitive coupling [4, 28, 34, 49–51], the system Hamiltonian is diagonal in the eigenbasis of the individual QD, represented as the tensor product of the number operator eigenstates. The four eigenstates $\{|0\rangle, |\downarrow\rangle\} \otimes \{|0\rangle, |\uparrow\rangle\}$, are labeled by $|\mathbb{A}\rangle = |00\rangle$, $|\mathbb{B}\rangle = |\downarrow 0\rangle$, $|\mathbb{C}\rangle = |0\uparrow\rangle$, $|\mathbb{D}\rangle = |\downarrow\uparrow\rangle$ with corresponding energies (ε_i , $i = \mathbb{A}, \mathbb{B}, \mathbb{C}, \mathbb{D}$): $\varepsilon_{\mathbb{A}} = 0$, $\varepsilon_{\mathbb{B}} = \varepsilon_L$, $\varepsilon_{\mathbb{C}} = \varepsilon_R$ and $\varepsilon_{\mathbb{D}} = \varepsilon_L + \varepsilon_R + \kappa$ [FIG. 1(b), 1(c)]. Here, $\varepsilon_L < \varepsilon_R$ is assumed w.l.o.g, while, κ_c and κ_s are non-negative, making the total interaction $\kappa = \kappa_c - \kappa_s$, either attractive (negative) or repulsive (positive). Notably, when $\kappa < 0$ and $|\kappa| > \varepsilon_L$ i.e. $-\kappa > \varepsilon_L > 0$, the energy states $|\mathbb{C}\rangle$ and $|\mathbb{D}\rangle$ swap their positions [FIG. 1(c)], a key factor leading

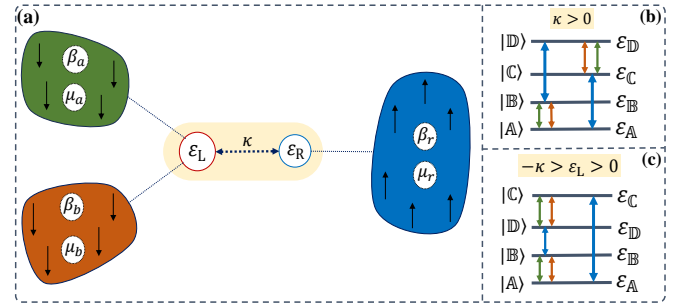


FIG. 1. (a) Schematic diagram of the three-terminal Coulomb-coupled QDs. The energy level diagram of the eigenstates of coupled QDs for (b) $\kappa > 0$ and (c) $\kappa < 0$; $|\kappa| > \varepsilon_L$ i.e. $-\kappa > \varepsilon_L > 0$.

to ICC behavior as we will discover in Sec. VII.

The reservoirs filled with fermionic particles (electrons) are characterized by temperature and chemical potential. The Hamiltonian for the λ 'th spin-polarized reservoir with spin $\sigma = \{\uparrow, \downarrow\}$, is defined as $H_B^\lambda \equiv H_B^{\lambda\sigma} = \sum_k (\varepsilon_k^{\lambda\sigma} - \mu_{\lambda\sigma}) c_{\lambda\sigma k}^\dagger c_{\lambda\sigma k}$, where $\varepsilon_k^{\lambda\sigma}$ is the energy of the non-interacting electrons, $\mu_{\lambda\sigma}$ is the chemical potential, and c^\dagger (c) are creation (annihilation) operators. The total reservoir Hamiltonian is $H_B = \sum_\lambda H_B^\lambda$. The QDs are weakly coupled to the reservoirs, enabling sequential tunneling [28, 31, 34, 40, 51], where only one QD interacts with the lead at a time. The tunnel-coupled Hamiltonians are characterized by the coupling constant $t_k^{\alpha\sigma\lambda}$ and are given by

$$H_T^{L\downarrow a(b)} = \hbar \sum_k [t_k^{L\downarrow a(b)} c_{a(b)\downarrow k}^\dagger d_{L\downarrow} + t_k^{L\downarrow a(b)*} d_{L\downarrow}^\dagger c_{a(b)\downarrow k}],$$

$$H_T^{R\uparrow r} = \hbar \sum_k [t_k^{R\uparrow r} c_{r\uparrow k}^\dagger d_{R\uparrow} + t_k^{R\uparrow r*} d_{R\uparrow}^\dagger c_{r\uparrow k}], \quad (2)$$

where, $H_T^{L\downarrow a(b)}$ describes the interaction between QD_L and reservoir $a(b)$ via \downarrow electrons and $H_T^{R\uparrow r}$ represents the interaction between QD_R and reservoir r via \uparrow electrons. Coulomb blockade and the sequential tunneling approximation prohibit transitions $|\mathbb{B}\rangle \leftrightarrow |\mathbb{C}\rangle$ and $|\mathbb{A}\rangle \leftrightarrow |\mathbb{D}\rangle$, allowing four allowed transitions. Reservoirs a, b control $|\mathbb{A}\rangle \leftrightarrow |\mathbb{B}\rangle$ and $|\mathbb{C}\rangle \leftrightarrow |\mathbb{D}\rangle$, while r governs $|\mathbb{A}\rangle \leftrightarrow |\mathbb{C}\rangle$ and $|\mathbb{B}\rangle \leftrightarrow |\mathbb{D}\rangle$ as demonstrated in FIG. 1(b), 1(c). Transition energies are defined as $\omega_{ij} = \varepsilon_j - \varepsilon_i$, with $\omega_{AB} = \varepsilon_L$, $\omega_{AC} = \varepsilon_R$, $\omega_{CD} = \varepsilon_L + \kappa$, and $\omega_{BD} = \varepsilon_R + \kappa$, evident from FIG. 1(b), 1(c). The Lindblad Master Equation (LME) under the Born-Markov approximation is used to analyze transition rates and system dynamics.

III. SYSTEM DYNAMICS

The composite system's state is represented by the reduced density matrix $\rho_s(t) = \text{Tr}_B\{\rho_{\text{tot}}(t)\}$, derived from the total density matrix $\rho_{\text{tot}}(t)$ of the system and bath. Using strong-coupling formalism, the time evolution of $\rho_s(t)$ is governed by the LME under the Born,

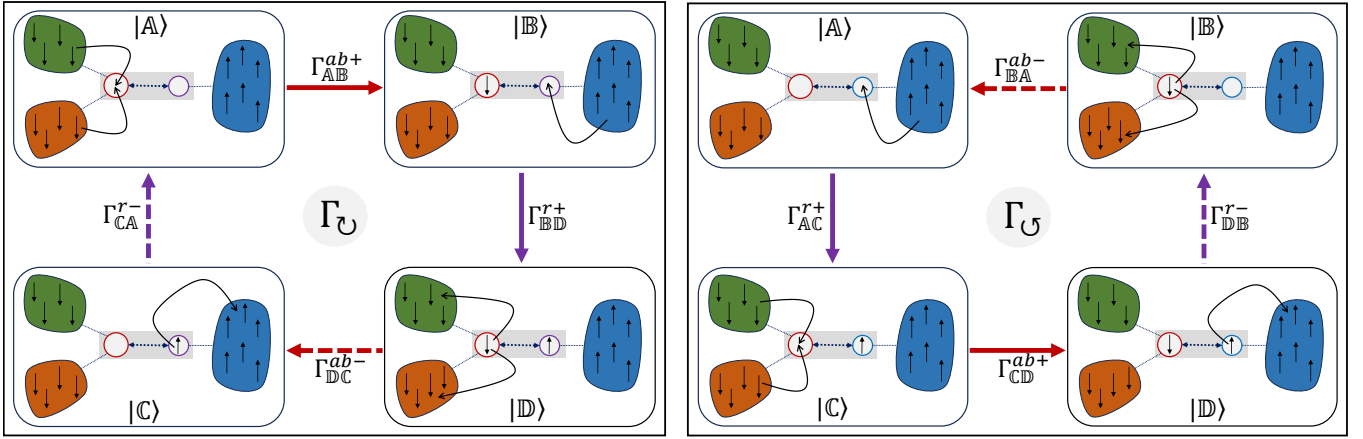


FIG. 2. Schematic representation of the clockwise (Left) and anti-clockwise (Right) transition cycles, induced by energy flow from one bath to another, associated with the particle exchange between QDs and the coupled reservoirs. At steady state, all transition rates of the clockwise (anti-clockwise) cycles are equal to each other and represented by Γ_O (Γ_O^r) [Cf. Eq. (16)].

Markov, and Secular (BMS) approximations [34, 51–53] (Appendix- A):

$$\frac{d}{dt}\rho_s(t) = \sum_{\lambda} \mathcal{L}_{\lambda}[\rho_s(t)]; \quad \lambda = a, b, r. \quad (3)$$

It is worth noting that the strong coupling formalism pertains to the interaction between QDs, while we still assume the weak coupling between the system and its

environment. This validates the use of the BMS approximation to derive the LME [Eq. (3)] based on the eigenstates of the system Hamiltonian H_s only. Consequently, each QD's dissipation depends on both its bath coupling and inter-QD interactions, which are crucial for accurately modeling heat flow across various system parameters. The Lindblad super-operator $\mathcal{L}_{\lambda}[\rho_s(t)]$ in Eq. (3) is defined as:

$$\mathcal{L}_{\lambda}[\rho_s(t)] = \sum_{\{\omega_{\alpha}\} > 0} \left\{ \gamma_{\lambda}(\omega_{\alpha}) f_{\lambda}^{+}(\omega_{\alpha}) \left[d_{\alpha\sigma}^{\dagger}(\omega_{\alpha}) \rho_s d_{\alpha\sigma}(\omega_{\alpha}) - \frac{1}{2} \{ \rho_s, d_{\alpha\sigma}^{\dagger}(\omega_{\alpha}) d_{\alpha\sigma}(\omega_{\alpha}) \} \right] \right. \\ \left. + \gamma_{\lambda}(\omega_{\alpha}) f_{\lambda}^{-}(\omega_{\alpha}) \left[d_{\alpha\sigma}(\omega_{\alpha}) \rho_s d_{\alpha\sigma}^{\dagger}(\omega_{\alpha}) - \frac{1}{2} \{ \rho_s, d_{\alpha\sigma}^{\dagger}(\omega_{\alpha}) d_{\alpha\sigma}(\omega_{\alpha}) \} \right] \right\}. \quad (4)$$

The bare electron transfer rate $\gamma_{\lambda}(\omega_{\alpha})$ between reservoir λ and QD $_{\alpha}$ is given by Fermi's golden rule $\gamma_{\lambda}(\omega_{\alpha}) \equiv \gamma_{\lambda\sigma}(\omega_{\alpha}) = 2\pi \sum_k |t_k^{\alpha\sigma\lambda}|^2 \delta(\omega_{\alpha} - \epsilon_k^{\lambda\sigma})$, where ω_{α} is the energy associated with transitions between QD $_{\alpha}$ and its coupled lead. For simplicity, we write $\gamma_{a(b)}(\omega_L) \equiv \gamma_{a(b)}$ and $\gamma_r(\omega_R) \equiv \gamma_r$, where $\omega_L = \{\omega_{AB}, \omega_{CD}\}$ and $\omega_R = \{\omega_{AC}, \omega_{BD}\}$, for excitation (particle is entering into the system), and similarly for de-excitation (particle leaving from the system) [FIG. 2].

To simplify calculations without relying on the specific ordering of system eigen-energies, we define the Fermi distribution function (FDF), $f_{\lambda}^{\pm}(\omega_{ij})$ governing transitions $|i\rangle \rightarrow |j\rangle$. The '+' sign represents excitation (particle entering the system), while '-' indicates de-excitation (particle leaving from the system) [4, 6], which is explicitly evident from the FIG. 2. This notation is independent of eigenstate arrangements and satisfies the rela-

tion [33, 34]:

$$f_{\lambda}^{+}(\omega_{ij}) = 1 - f_{\lambda}^{-}(\omega_{ij}) = \left[1 + \exp \left(\frac{\omega_{ij} - \mu_{\lambda}}{k_B T_{\lambda}} \right) \right]^{-1}, \quad (5)$$

where T_{λ} and μ_{λ} are the temperature and chemical potential of the λ -th reservoir. From FIG. 2 and Eq. (4), the rate equations for occupation probabilities are:

$$\dot{\rho}_A = -\Gamma_{AB}^{ab+} - \Gamma_{AC}^{r+}; \quad \dot{\rho}_B = \Gamma_{AB}^{ab+} - \Gamma_{BD}^{r+}; \\ \dot{\rho}_C = -\Gamma_{CD}^{ab+} + \Gamma_{AC}^{r+}; \quad \dot{\rho}_D = \Gamma_{CD}^{ab+} + \Gamma_{BD}^{r+}, \quad (6)$$

where, $\dot{\rho}_i = \sum_{\lambda=a,b,r} \langle i | \mathcal{L}_{\lambda}[\rho_s(t)] | i \rangle$ and $\Gamma_{ij}^{ab\pm} \equiv \Gamma_{ij}^{a\pm} + \Gamma_{ij}^{b\pm}$. The net transition rate $\Gamma_{ij}^{\lambda\pm}$ mediated by reservoir λ is expressed as:

$$\Gamma_{ij}^{\lambda\pm} \equiv \Gamma_{i\rightarrow j}^{\lambda\pm} = k_{ij}^{\lambda\pm} \rho_i - k_{ji}^{\lambda\mp} \rho_j \quad (7)$$

where

$$k_{ij}^{\lambda\pm} = \gamma_{\lambda} f_{\lambda}^{\pm}(\omega_{ij}) \quad ; \quad k_{ji}^{\lambda\mp} = \gamma_{\lambda} f_{\lambda}^{\mp}(\omega_{ji}). \quad (8)$$

For fermionic reservoirs:

$$k_{ij}^{\lambda\pm} + k_{ji}^{\lambda\mp} = \gamma_\lambda. \quad (9)$$

Assuming all γ_λ are equal, we derive closed-form expressions for steady-state energy and particle currents in Sec. IV.

IV. STEADY STATE CURRENTS

To derive the expressions for steady-state currents under the grand canonical formalism, we consider the equilibrium initial density operator of the system $\rho_s(0)$ as [53]

$$\rho_s^{\text{eq}} = \rho_s(0) = \frac{e^{-\bar{\beta}(H_s - \bar{\mu}\mathcal{N})}}{\mathcal{Z}(\bar{\beta}, \bar{\mu})}, \quad (10)$$

where $\mathcal{Z}(\bar{\beta}, \bar{\mu}) = \text{Tr} \left[e^{-\bar{\beta}(H_s - \bar{\mu}\mathcal{N})} \right]$ is the grand canonical partition function and $\mathcal{N} = \mathcal{N}_{L\downarrow} + \mathcal{N}_{R\uparrow}$ being the total particle number operator of the two QDs. The $\bar{\beta}$ and $\bar{\mu}$ are the effective inverse temperature and chemical potential, $\bar{\beta} = \sum_\lambda \beta_\lambda$ and $\bar{\mu} = \sum_\lambda \mu_\lambda$ respectively. We assume that environmental interaction slightly perturbs the system from its initial equilibrium state $\rho_s(0) = \rho_s^{\text{eq}}$ to $\rho_s(t)$, such that $\delta\rho_s(t) = \rho_s(t) - \rho_s(0) \equiv \mathcal{O}(\xi)$, where ξ is a small expansion parameter. Following Ref. [53], equating system von-Neumann entropy (times k_B) with thermodynamic entropy near close to equilibrium [54–56]

$$\mathcal{S}_s(t) = -k_B \text{Tr}_s[\rho_s(t) \ln \rho_s(t)], \quad (11)$$

and retaining only terms that are first order in ξ , the expression for $\Delta\mathcal{S}_s = \mathcal{S}_s(t) - \mathcal{S}_s(0)$ can be derived as [53]

$$\begin{aligned} \Delta\mathcal{S}_s(t) &\approx -k_B \text{Tr}_s[\delta\rho_s(t) \ln \rho_s^{\text{eq}}] \\ &= k_B \beta \text{Tr}_s[\delta\rho_s(t) H_s] - k_B \beta \mu \text{Tr}_s[\delta\rho_s(t) \mathcal{N}]. \end{aligned} \quad (12)$$

Comparing Eq. (12) and the first law of thermodynamics in the presence of *chemical work done*, we identify change in energy as $\Delta E = \text{Tr}_s[\delta\rho_s(t) H_s]$ and change in particles number as $\Delta N = \text{Tr}_s[\delta\rho_s(t) \mathcal{N}]$. Noting $\delta\rho_s(t) = \rho_s(t) - \rho_s(0)$, and H_s, \mathcal{N} are time-independent, the net energy flux (J_E) and particle flux (J_N) are recognized as follows:

$$\begin{aligned} J_E(t) &= \text{Tr}_s[\dot{\rho}_s(t) H_s] = \sum_{\lambda=a,b,r} \text{Tr}_s[\mathcal{L}_\lambda[\rho_s(t)] H_s], \\ J_N(t) &= \text{Tr}_s[\dot{\rho}_s(t) \mathcal{N}] = \sum_{\lambda=a,b,r} \text{Tr}_s[\mathcal{L}_\lambda[\rho_s(t)] \mathcal{N}], \end{aligned} \quad (13)$$

where we use Eq. (3) for $\dot{\rho}_s(t)$. Identifying $J_{E(N)}$ as the sum of the contributions of energy (particle) flux associated with all three reservoirs: $J_E(t) = \sum_\lambda J_E^\lambda(t)$; $J_N(t) = \sum_\lambda J_N^\lambda(t)$, where $J_{E(N)}^\lambda$ is positive if energy (particle) current flows from the reservoir λ to the system, we obtain

$$J_E^\lambda(t) = \text{Tr}_s[\mathcal{L}_\lambda[\rho(t)] H_s]; J_N^\lambda(t) = \text{Tr}_s[\mathcal{L}_\lambda[\rho(t)] \mathcal{N}]. \quad (14)$$

The heat current is obtained as $J_Q^\lambda(t) = J_E^\lambda(t) - \mu_\lambda J_N^\lambda(t)$, which at steady state simplifies to $J_Q^\lambda = J_E^\lambda - \mu_\lambda J_N^\lambda$. Here $J_E^\lambda = \text{Tr}_s[\mathcal{L}_\lambda[\rho_{ss}] H_s]$ and $J_N^\lambda = \text{Tr}_s[\mathcal{L}_\lambda[\rho_{ss}] \mathcal{N}]$. Using Eq. (4) for the $\mathcal{L}_\lambda[\rho_{ss}]$, all three steady state currents are given by [57]:

$$\begin{aligned} J_E^\lambda &= \sum_{\{\omega_{ij}\}} \omega_{ij} \Gamma_{ij}^{\lambda+} = \sum_{\{\omega_{ji}\}} \omega_{ji} \Gamma_{ji}^{\lambda-}; \\ J_N^\lambda &= \sum_{\{\omega_{ij}\}} \Gamma_{ij}^{\lambda+} = \sum_{\{\omega_{ji}\}} \Gamma_{ji}^{\lambda-}; \\ J_Q^\lambda &= \sum_{\{\omega_{ij}\}} (\omega_{ij} - \mu_\lambda) \Gamma_{ij}^{\lambda+} = \sum_{\{\omega_{ji}\}} (\omega_{ji} - \mu_\lambda) \Gamma_{ji}^{\lambda-}, \end{aligned} \quad (15)$$

where we use the relation $\Gamma_{ij}^{\lambda+} = -\Gamma_{ji}^{\lambda-}$. The explicit expressions for all three currents are given in Appendix-B. At steady state ($\dot{\rho}_i = 0$), the transition rates satisfy:

$$\begin{aligned} \Gamma_{AB}^{ab+} &= \Gamma_{BD}^{r+} = \Gamma_{DC}^{ab-} = \Gamma_{CA}^{r-} = \Gamma_{ABCDA} \equiv \Gamma_O; \\ \Gamma_{AC}^{r+} &= \Gamma_{CD}^{ab+} = \Gamma_{DB}^{r-} = \Gamma_{BA}^{ab-} = \Gamma_{ACDBA} \equiv \Gamma_O, \end{aligned} \quad (16)$$

implying $\Gamma_O = -\Gamma_O$ [FIG. 2]. With the help of Eq. (15), one can verify

$$\begin{aligned} J_E^r &= \varepsilon_R \Gamma_O + (\varepsilon_R + \kappa) \Gamma_O = \kappa \Gamma_O; \\ J_N^r &= \Gamma_{AC}^{r+} + \Gamma_{BD}^{r+} = \Gamma_O + \Gamma_O = 0, \end{aligned} \quad (17)$$

as QD_R is coupled only to lead r , resulting in $J_N^r = 0$. This gives $J_Q^r = J_E^r = \kappa \Gamma_O$. However, QD_L is coupled to leads a and b , allowing steady state (spin-polarized) particle flow between them. Conservation of total energy and particle currents at steady state, $\sum_\lambda J_E^\lambda = 0$ and $\sum_\lambda J_N^\lambda = 0$ gives:

$$J_E^r = -J_E^{ab} = \kappa \Gamma_O; \quad J_N^a = -J_N^b. \quad (18)$$

The explicit form of Γ_O is provided in Appendix-C. Unlike energy, heat current is not conserved, as $J_Q^a + J_Q^b \equiv J_Q^{ab} \neq J_E^{ab} = -\kappa \Gamma_O$. Next, we discuss the connection between these currents and entropy production near equilibrium through thermodynamic force-flux relation.

V. THERMODYNAMIC FORCE, FLUX AND ENTROPY PRODUCTION RATE

From Eq. (12), one can write [56]

$$\Delta\mathcal{S}_s(t) = \Sigma(t) + \Phi(t), \quad (19)$$

where $\Sigma(t)$ is the *entropy production* and $\Phi(t)$ is the *entropy flux*. The explicit forms of $\Sigma(t)$ and the $\Phi(t)$ are derived following Refs. [55, 56] [See Appendix-D]:

$$\begin{aligned} \Sigma(t) &= k_B \text{Tr}[\rho_{\text{tot}}(t) \ln \{\rho_{\text{tot}}(t)\}] \\ &\quad - k_B \text{Tr} \left[\rho_{\text{tot}}(t) \ln \left\{ \rho_s(t) \prod_\lambda \rho_\lambda^{\text{eq}} \right\} \right], \\ \Phi(t) &= k_B \sum_\lambda \text{Tr}_\lambda [\{\rho_\lambda(t) - \rho_\lambda^{\text{eq}}\} \ln \rho_\lambda^{\text{eq}}], \end{aligned} \quad (20)$$

where, ρ_λ^{eq} and $\rho_\lambda(t)$ are the equilibrium and *near equilibrium* density operators of reservoir λ , respectively. In the grand canonical ensemble, ρ_λ^{eq} is expressed as:

$$\rho_\lambda^{\text{eq}} = \frac{e^{-\beta_\lambda H_B^\lambda}}{\mathcal{Z}_\lambda(\beta_\lambda)}, \quad (21)$$

where $H_B^\lambda \equiv H_B^{\lambda\sigma} = \sum_k (\epsilon_k^{\lambda\sigma} - \mu_{\lambda\sigma}) c_{\lambda\sigma k}^\dagger c_{\lambda\sigma k}$ and $\mathcal{Z}_\lambda(\beta_\lambda) = \text{Tr}[e^{-\beta_\lambda H_B^\lambda}]$ is the the grand canonical partition function. As a result, $\Phi(t)$ is identified as the reversible heat exchanged with the reservoir between some final and initial times

$$\Phi(t) = -k_B \sum_\lambda \beta_\lambda [\langle H_B^\lambda \rangle_t - \langle H_B^\lambda \rangle_0] = k_B \sum_\lambda \beta_\lambda \Delta Q_\lambda, \quad (22)$$

where $\Delta Q_\lambda = \langle H_B^\lambda \rangle_0 - \langle H_B^\lambda \rangle_t$ and $\langle H_B^\lambda \rangle_t = \text{Tr}_\lambda[\rho_\lambda(t) H_B^\lambda]$. Thus, we rewrite Eq. (19) as

$$\Delta S_s(t) = \Sigma(t) + k_B \sum_\lambda \beta_\lambda \Delta Q_\lambda, \quad (23)$$

where we replace the second term by Eq. (22). At steady state, the system's entropy remains constant, i.e., $\frac{d}{dt} \{\Delta S_s(t)\} = 0$, and $\dot{\Sigma}$ reaches its minimum [53, 55, 56]. So, Eq. (23) yields

$$\dot{\Sigma} = -k_B \sum_\lambda \beta_\lambda \frac{d}{dt} \{\Delta Q_\lambda\} = -k_B \sum_\lambda \beta_\lambda J_\lambda^\lambda. \quad (24)$$

Substituting $J_\lambda^\lambda = J_E^\lambda - \mu_\lambda J_N^\lambda$ into Eq. (24), the entropy production rate for the three-terminal system becomes:

$$\dot{\Sigma} = J_E^r \mathcal{F}_E^r + J_E^b \mathcal{F}_E^b + J_N^b \mathcal{F}_N^b, \quad (25)$$

where, $J_N^r = 0$ (from Eq. (17)) and we utilize energy and particle current conservation laws $J_E = \sum_\lambda J_E^\lambda = 0$ and $J_N = \sum_\lambda J_N^\lambda = 0$. The thermodynamic forces conjugate

to the fluxes $\{J_E^r, J_E^b, J_N^b\}$ in Eq. (25) are:

$$\begin{aligned} \mathcal{F}_E^r &= k_B(\beta_a - \beta_r); \\ \mathcal{F}_E^b &= k_B(\beta_a - \beta_b); \\ \mathcal{F}_N^b &= k_B(\beta_b \mu_b - \beta_a \mu_a). \end{aligned} \quad (26)$$

It is evident from Eq. (26) that, for positive values, \mathcal{F}_E^b and \mathcal{F}_N^b are two mutually parallel forces, while \mathcal{F}_E^r is not.

Though Eq. (25) links the entropy production rate to the *complete set* of macroscopic thermodynamic forces and fluxes via temperature, chemical potential, and amount of heat exchange with the reservoirs, to grasp the full essence of thermodynamic principles of inverse current, we must identify the microscopic descriptions of these thermodynamic quantities. The ideal starting point could be the entropy production rate, which sets the connection between macroscopic and microscopic thermodynamic frameworks. So, rewriting the von-Neumann entropy defined in Eq. (11)

$$S_s(t) = -k_B \sum_i \rho_i(t) \ln \rho_i(t), \quad (27)$$

in terms of the microscopic populations of the different system eigenstates, $\{\rho_i\}$ ($i = \mathbb{A}, \mathbb{B}, \mathbb{C}, \mathbb{D}$), we evaluate the time evolution of the system's entropy change as [54]

$$\begin{aligned} \frac{d}{dt} \Delta S_s(t) &= k_B \left[\Gamma_{\mathbb{A}\mathbb{B}}^{a+} \ln \left(\frac{\rho_{\mathbb{A}}}{\rho_{\mathbb{B}}} \right) + \Gamma_{\mathbb{A}\mathbb{B}}^{b+} \ln \left(\frac{\rho_{\mathbb{A}}}{\rho_{\mathbb{B}}} \right) + \Gamma_{\mathbb{B}\mathbb{D}}^{r+} \ln \left(\frac{\rho_{\mathbb{B}}}{\rho_{\mathbb{D}}} \right) \right. \\ &\quad \left. + \Gamma_{\mathbb{D}\mathbb{C}}^{a-} \ln \left(\frac{\rho_{\mathbb{D}}}{\rho_{\mathbb{C}}} \right) + \Gamma_{\mathbb{D}\mathbb{C}}^{b-} \ln \left(\frac{\rho_{\mathbb{D}}}{\rho_{\mathbb{C}}} \right) + \Gamma_{\mathbb{C}\mathbb{A}}^{r-} \ln \left(\frac{\rho_{\mathbb{C}}}{\rho_{\mathbb{A}}} \right) \right], \end{aligned} \quad (28)$$

where we use $\dot{\rho}_i(t)$ from Eq. (6) [See Appendix- E]. Comparing the above equation with Eq. (19), we identify the microscopic version of the entropy production rate and entropy flux [28, 54], as follows [Appendix- E]

$$\begin{aligned} \dot{\Sigma}(t) &= k_B \left[(k_{\mathbb{A}\mathbb{B}}^{a+} \rho_{\mathbb{A}} - k_{\mathbb{B}\mathbb{A}}^{a-} \rho_{\mathbb{B}}) \ln \left(\frac{k_{\mathbb{A}\mathbb{B}}^{a+} \rho_{\mathbb{A}}}{k_{\mathbb{B}\mathbb{A}}^{a-} \rho_{\mathbb{B}}} \right) + (k_{\mathbb{A}\mathbb{B}}^{b+} \rho_{\mathbb{A}} - k_{\mathbb{B}\mathbb{A}}^{b-} \rho_{\mathbb{B}}) \ln \left(\frac{k_{\mathbb{A}\mathbb{B}}^{b+} \rho_{\mathbb{A}}}{k_{\mathbb{B}\mathbb{A}}^{b-} \rho_{\mathbb{B}}} \right) + (k_{\mathbb{B}\mathbb{D}}^{r+} \rho_{\mathbb{B}} - k_{\mathbb{D}\mathbb{B}}^{r-} \rho_{\mathbb{D}}) \ln \left(\frac{k_{\mathbb{B}\mathbb{D}}^{r+} \rho_{\mathbb{B}}}{k_{\mathbb{D}\mathbb{B}}^{r-} \rho_{\mathbb{D}}} \right) \right. \\ &\quad \left. + (k_{\mathbb{D}\mathbb{C}}^{a-} \rho_{\mathbb{D}} - k_{\mathbb{C}\mathbb{D}}^{a+} \rho_{\mathbb{C}}) \ln \left(\frac{k_{\mathbb{D}\mathbb{C}}^{a-} \rho_{\mathbb{D}}}{k_{\mathbb{C}\mathbb{D}}^{a+} \rho_{\mathbb{C}}} \right) + (k_{\mathbb{D}\mathbb{C}}^{b-} \rho_{\mathbb{D}} - k_{\mathbb{C}\mathbb{D}}^{b+} \rho_{\mathbb{C}}) \ln \left(\frac{k_{\mathbb{D}\mathbb{C}}^{b-} \rho_{\mathbb{D}}}{k_{\mathbb{C}\mathbb{D}}^{b+} \rho_{\mathbb{C}}} \right) + (k_{\mathbb{C}\mathbb{A}}^{r-} \rho_{\mathbb{C}} - k_{\mathbb{A}\mathbb{C}}^{r+} \rho_{\mathbb{A}}) \ln \left(\frac{k_{\mathbb{C}\mathbb{A}}^{r-} \rho_{\mathbb{C}}}{k_{\mathbb{A}\mathbb{C}}^{r+} \rho_{\mathbb{A}}} \right) \right], \\ \dot{\Phi}(t) &= -k_B \left[\Gamma_{\mathbb{A}\mathbb{B}}^{a+} \ln \left(\frac{k_{\mathbb{A}\mathbb{B}}^{a+}}{k_{\mathbb{B}\mathbb{A}}^{a-}} \right) + \Gamma_{\mathbb{A}\mathbb{B}}^{b+} \ln \left(\frac{k_{\mathbb{A}\mathbb{B}}^{b+}}{k_{\mathbb{B}\mathbb{A}}^{b-}} \right) + \Gamma_{\mathbb{B}\mathbb{D}}^{r+} \ln \left(\frac{k_{\mathbb{B}\mathbb{D}}^{r+}}{k_{\mathbb{D}\mathbb{B}}^{r-}} \right) + \Gamma_{\mathbb{D}\mathbb{C}}^{a-} \ln \left(\frac{k_{\mathbb{D}\mathbb{C}}^{a-}}{k_{\mathbb{C}\mathbb{D}}^{a+}} \right) + \Gamma_{\mathbb{D}\mathbb{C}}^{b-} \ln \left(\frac{k_{\mathbb{D}\mathbb{C}}^{b-}}{k_{\mathbb{C}\mathbb{D}}^{b+}} \right) + \Gamma_{\mathbb{C}\mathbb{A}}^{r-} \ln \left(\frac{k_{\mathbb{C}\mathbb{A}}^{r-}}{k_{\mathbb{A}\mathbb{C}}^{r+}} \right) \right]. \end{aligned} \quad (29)$$

In Eq. (29), each term of the Schnakenberg entropy production rate $\dot{\Sigma}$ [54], has the form $(a - b) \ln \left(\frac{a}{b} \right)$, ensuring

non-negativity of the total entropy production rate. At steady state, this leads to [Appendix- E]

$$\dot{\Sigma}(t) = -\dot{\Phi}(t) = \kappa \Gamma_{\circlearrowleft} \left[\left(\frac{k_B}{\kappa} \right) \ln \left(\frac{k_{AB}^{a+} k_{BD}^{r+} k_{DC}^{a-} k_{CA}^{r-}}{k_{BA}^{a-} k_{DB}^{r-} k_{CD}^{a+} k_{AC}^{r+}} \right) \right] + (\varepsilon_L \Gamma_{AB}^{b+} - (\varepsilon_L + \kappa) \Gamma_{DC}^{b-}) \left[\left(\frac{k_B}{\kappa} \right) \ln \left(\frac{k_{BA}^{b-} k_{AB}^{a+} k_{CD}^{b+} k_{DC}^{a-}}{k_{DC}^{b-} k_{CD}^{a+} k_{AB}^{b+} k_{BA}^{a-}} \right) \right] + (\Gamma_{AB}^{b+} - \Gamma_{DC}^{b-}) \left[k_B (1 + \theta) \ln \left(\frac{k_{AB}^{b+} k_{BA}^{a-}}{k_{BA}^{b-} k_{AB}^{a+}} \right) + k_B \theta \ln \left(\frac{k_{DC}^{b-} k_{CD}^{a+}}{k_{CD}^{b+} k_{DC}^{a-}} \right) \right] \equiv J_E^r \mathcal{F}_E^r + J_E^b \mathcal{F}_E^b + J_N^b \mathcal{F}_N^b, \quad (30)$$

where $\theta = (\frac{\varepsilon_L}{\kappa})$ is the scaled system parameter. The sign of θ plays a crucial role in determining the ICC behavior in energy and (spin-polarized) particle currents, as discussed in Sec. VII. From the above equation, all associated fluxes and their conjugate forces are identified as follows:

$$\begin{aligned} J_E^r &= \kappa \Gamma_{\circlearrowleft} ; \quad J_N^b = (\Gamma_{AB}^{b+} - \Gamma_{DC}^{b-}), \\ J_E^b &= \varepsilon_L \Gamma_{AB}^{b+} + (\varepsilon_L + \kappa) \Gamma_{CD}^{b-} = \varepsilon_L J_N^b + \kappa \Gamma_{CD}^{b-}, \end{aligned} \quad (31)$$

and

$$\mathcal{F}_E^r = \left(\frac{k_B}{\kappa} \right) \ln \left(\frac{k_{AB}^{a+} k_{BD}^{r+} k_{DC}^{a-} k_{CA}^{r-}}{k_{BA}^{a-} k_{DB}^{r-} k_{CD}^{a+} k_{AC}^{r+}} \right) = k_B (\beta_a - \beta_r), \quad (32a)$$

$$\mathcal{F}_E^b = \left(\frac{k_B}{\kappa} \right) \ln \left(\frac{k_{BA}^{b-} k_{AB}^{a+} k_{CD}^{b+} k_{DC}^{a-}}{k_{DC}^{b-} k_{CD}^{a+} k_{AB}^{b+} k_{BA}^{a-}} \right) = k_B (\beta_a - \beta_b), \quad (32b)$$

$$\begin{aligned} \mathcal{F}_N^b &= k_B (\theta + 1) \ln \left(\frac{k_{AB}^{b+} k_{BA}^{a-}}{k_{BA}^{b-} k_{AB}^{a+}} \right) + k_B \theta \ln \left(\frac{k_{DC}^{b-} k_{CD}^{a+}}{k_{CD}^{b+} k_{DC}^{a-}} \right) \\ &= k_B \ln \left(\frac{k_{AB}^{b+} k_{BA}^{a-}}{k_{BA}^{b-} k_{AB}^{a+}} \right) - \varepsilon_L \mathcal{F}_E^b = k_B (\beta_b \mu_b - \beta_a \mu_a) \end{aligned} \quad (32c)$$

Equation (31) is identical to Eq. (26). The equivalence between macroscopic and microscopic expressions of the above forces [Cf. Eq. (32)] can be verified using Eq. (8), and the corresponding FDFs. Equations (31)-(32) are the first major results of our analysis that follow the linearity of the underlying quantum master equation [Cf. Eq. (6)]. However, the presence of three force-flux pairs complicates analysis in a three-terminal model. As previously argued, ICC is a coupled transport phenomenon requiring only two parallel forces. By setting one particular energy force to zero, we identify two mutually parallel thermodynamic forces (one energy and one particle force), meeting the minimal criteria to study ICC.

VI. NORMAL CROSS-EFFECT VS ICC

To differentiate ICC and normal cross-effect in a coupled transport, we have to reduce the three-terminal model such that the non-zero forces remain parallel to each other and, this can be achieved by setting the force \mathcal{F}_E^r zero in Eq. (32). Considering $\beta_a = \beta_r$, we can set $\mathcal{F}_E^r = 0$ which modifies Eq. (30) as $\dot{\Sigma} = J_E^b \mathcal{F}_E^b + J_N^b \mathcal{F}_N^b$,

where both forces are mutually parallel. According to Wang *et al.* [3], it is necessary to consider the expressions of the entropy production rate in which all forces should be mutually parallel so that ICC and normal cross-effects can be distinguished unambiguously. For ICC in the energy (particle) current, $J_{E(N)}^b < 0$, when both $\mathcal{F}_E^b > 0$ and $\mathcal{F}_N^b > 0$ [FIG. 3]. In the case of normal cross-effect, \mathcal{F}_E^b and \mathcal{F}_N^b have opposite signs as they oppose each other. In other words, when two thermodynamic forces appearing in the entropy production rate have the same sign, they do not oppose each other in the case of ICC, unlike in the normal cross-effect where they do. Hence, the cross-effect in the energy (particle) current can be described by the condition $J_{E(N)}^b < 0$, when the conjugate force $\mathcal{F}_{E(N)}^b > 0$ but the non-conjugate force $\mathcal{F}_{N(E)}^b < 0$ [FIG. 3].

Finally, it is evident from Eq. (32) that the thermodynamic forces and gradients are not always equivalent. While \mathcal{F}_E aligns with ΔT (upto a normalization), equating $\Delta\mu$ with \mathcal{F}_N is misleading, since \mathcal{F}_N and $\Delta\mu$ can have even opposite signs. For example, \mathcal{F}_N^b in Eq. (32c) and

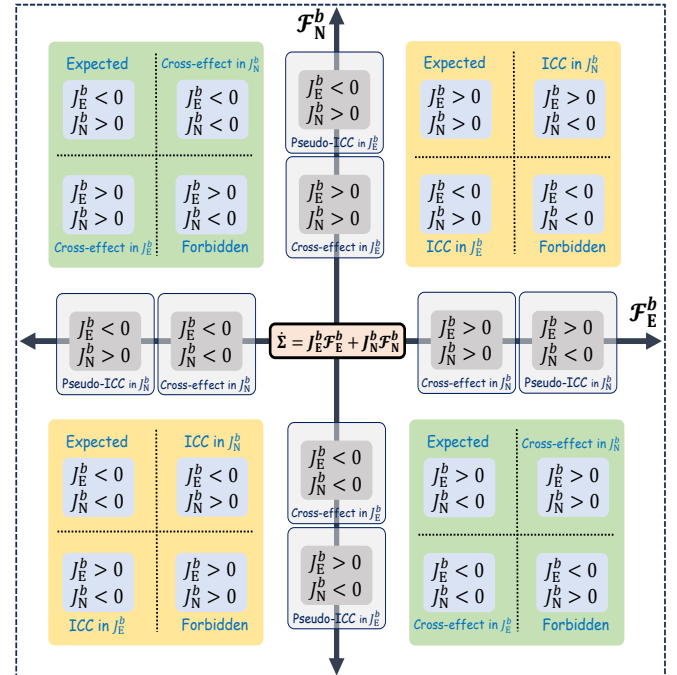


FIG. 3. Pictorial representation of various thermodynamic phenomena governed by the entropy production rate $\dot{\Sigma} = J_E^b \mathcal{F}_E^b + J_N^b \mathcal{F}_N^b$ i.e., normal cross-effect, ICC (yellow shaded), and pseudo-ICC phenomena.

the chemical potential gradient $\Delta\mu = \mu_b - \mu_a$ are not identical unless $\beta_a = \beta_b$. Consequently, relying solely on $\Delta\mu > 0$ risks misinterpreting a normal cross-effect as ICC. This issue arises in the analysis of the two-terminal ICC model by Zhang *et al.* [4]. While their results show a current opposing both gradients (ΔT and $\Delta\mu$), this behavior does not necessarily qualify as genuine ICC.

Now, a note on the term “pseudo-ICC” is appropriate here. In this case, one force is set to zero (i.e., it lacks a specific direction), causing the conjugate flux to be unaffected by its corresponding force. Then, the current can flow along or against the non-conjugate force, both being thermodynamically allowed. If the flux opposes the applied force by having an opposite sign to the non-conjugate force, we call it pseudo-ICC [FIG. 3], as it lacks a conjugate force and represents a *special* type of ICC. While achieving genuine ICC is a challenging task, pseudo-ICC could serve as a preliminary indicator.

In a nutshell, considering the definition of the entropy production rate as $\dot{\Sigma} = J_E^b \mathcal{F}_E^b + J_N^b \mathcal{F}_N^b$, all probable outcomes under four co-ordinates of $(\mathcal{F}_E^b, \mathcal{F}_N^b)$ can be depicted pictorially in FIG.3. It is clear from FIG.3 that ICC can be obtained in the first and third quadrants, whereas to observe a cross-effect, one must consider the second or fourth quadrants.

VII. EXAMINING ICC: RESULT AND DISCUSSION

As discussed in the previous section, by considering $\beta_a = \beta_r = \beta$, we can set the non-parallel force \mathcal{F}_r^r to zero, consequently our three-terminal model reduces to an ideal coupled transport model with two parallel force-flux pairs, with $\mathcal{F}_E^b = k_B(\beta - \beta_b)$ and $\mathcal{F}_N^b = k_B(\beta_b \mu_b - \beta \mu_a)$. We will now analyze the model with the above two parallel forces and their conjugate fluxes. For all numerical plots, we have considered $\gamma_a \simeq \gamma_b \simeq \gamma_r \equiv \gamma$ and plotted appropriately scaled dimensionless forces and fluxes. Since the ICC can be obtained only in the first and third quadrants [FIG. 3], the scaled forces are taken either zero or positive w.l.o.g, i.e., we will consider only the first quadrant.

A. Setting both forces zero

When both forces $(\mathcal{F}_E^b, \mathcal{F}_N^b) = 0$, the currents (J_E^b, J_N^b) vanish, as can be demonstrated analytically using microscopic expressions of forces. Setting $(\mathcal{F}_E^b, \mathcal{F}_N^b) = 0$, in Eq. (32c) yields:

$$\left(\frac{k_{AB}^{b+} k_{BA}^{a-}}{k_{BA}^{b-} k_{AB}^{a+}} \right) = 1. \quad (33)$$

With $\mathcal{F}_E^b = 0$, it further follows from Eq. (32b)

$$\left(\frac{k_{AB}^{b+} k_{BA}^{a-}}{k_{BA}^{b-} k_{AB}^{a+}} \right) = \left(\frac{k_{CD}^{b+} k_{DC}^{a-}}{k_{DC}^{b-} k_{CD}^{a+}} \right) = 1. \quad (34)$$

With the help of Eq. (9), above equation simplifies to:

$$\begin{aligned} \left(\frac{k_{AB}^{b+}}{k_{BA}^{b-}} \right) &= \left(\frac{k_{AB}^{a+}}{k_{BA}^{a-}} \right) = \left(\frac{k_{AB}^{ab+}}{k_{BA}^{ab-}} \right), \\ \left(\frac{k_{CD}^{b+}}{k_{DC}^{b-}} \right) &= \left(\frac{k_{CD}^{a+}}{k_{DC}^{a-}} \right) = \left(\frac{k_{CD}^{ab+}}{k_{DC}^{ab-}} \right). \end{aligned} \quad (35)$$

Using the above relations in Eq. (7), we obtain

$$\Gamma_{AB}^{ab+} = 2\Gamma_{AB}^{a+} = 2\Gamma_{AB}^{b+}; \quad \Gamma_{CD}^{ab+} = 2\Gamma_{CD}^{a+} = 2\Gamma_{CD}^{b+}. \quad (36)$$

Combining this with Eq. (16) gives $\Gamma_{AB}^{b+} = -\Gamma_{CD}^{b+}$. Consequently, from Eq. (31), the spin-polarized particle current $J_N^b = 0$, reducing the relation to $J_E^b = \kappa\Gamma_{CD}^{b+}$. Using Eq. (36) with Eq. (16), this simplifies to $J_E^b = \frac{1}{2}\kappa\Gamma_{\circlearrowleft}$. As $\mathcal{F}_E^r = 0$, Eq. (32a) further yields:

$$\left(\frac{k_{AB}^{a+} k_{BD}^{r+} k_{DC}^{a-} k_{CA}^{r-}}{k_{BA}^{a-} k_{DB}^{r-} k_{CD}^{a+} k_{AC}^{r+}} \right) = 1. \quad (37)$$

Using the relation in Eq. (34), we can express

$$\left(\frac{k_{AB}^{ab+} \rho_A}{k_{BA}^{ab-} \rho_B} \right) \left(\frac{k_{BD}^{r+} \rho_B}{k_{DB}^{r-} \rho_D} \right) \left(\frac{k_{DC}^{ab-} \rho_D}{k_{CD}^{ab+} \rho_C} \right) \left(\frac{k_{CA}^{r-} \rho_C}{k_{AC}^{r+} \rho_A} \right) = 1. \quad (38)$$

At steady state, each term within the parenthesis must equal 1 to satisfy this condition. Applying this to Eqs. (7) and (16), we find, $\Gamma_{\circlearrowleft} = \Gamma_{\circlearrowright} = 0$, leading to Eq. (31) as $J_E^r = \kappa\Gamma_{\circlearrowleft} = 0$. Consequently, the energy current reduces to, $J_E^b = \frac{1}{2}\kappa\Gamma_{\circlearrowleft} = 0$. Thus, both fluxes, $(J_E^b$ and $J_N^b)$, vanish as the forces $(\mathcal{F}_E^b, \mathcal{F}_N^b)$, are zero.

B. Examining pseudo-ICC: When one force is zero

We will now examine pseudo-ICC in particle and energy currents, by setting \mathcal{F}_N^b and \mathcal{F}_E^b to zero, respectively.

1. Setting \mathcal{F}_N^b as zero: pseudo-ICC in J_N^b

With $\mathcal{F}_N^b = 0$ and $\mathcal{F}_E^b > 0$, we focus on the first quadrant of FIG. 3 where $\dot{\Sigma} = J_E^b \mathcal{F}_E^b$, ensuring that J_E^b aligns with \mathcal{F}_E^b to maintain $\dot{\Sigma} \geq 0$. Under these conditions, after a little bit of algebra, Eq. (32c) for the particle force simplifies to

$$\ln \left(\frac{k_{AB}^{b+} k_{BA}^{a-}}{k_{BA}^{b-} k_{AB}^{a+}} \right) = \left(\frac{\theta}{1+\theta} \right) \ln \left(\frac{k_{CD}^{b+} k_{DC}^{a-}}{k_{DC}^{b-} k_{CD}^{a+}} \right) > 0, \quad (39)$$

where, $\left(\frac{\theta}{1+\theta} \right) = \left(\frac{\varepsilon_L}{\varepsilon_L + \kappa} \right)$. This leads to two possible cases:

- For $\kappa > 0$, the above relation simplifies to,

$$\left(\frac{k_{AB}^{b+} k_{BA}^{a-}}{k_{BA}^{b-} k_{AB}^{a+}} \right) > 1 \quad ; \quad \left(\frac{k_{CD}^{b+} k_{DC}^{a-}}{k_{DC}^{b-} k_{CD}^{a+}} \right) > 1, \quad (40)$$

which directly implies

$$\left(\frac{k_{AB}^{b+}}{k_{BA}^{b-}} \right) > \left(\frac{k_{AB}^{a+}}{k_{BA}^{a-}} \right) \quad ; \quad \left(\frac{k_{CD}^{b+}}{k_{DC}^{b-}} \right) > \left(\frac{k_{CD}^{a+}}{k_{DC}^{a-}} \right). \quad (41)$$

Applying Eq. (9) to Eq. (41), we get $k_{BA(DC)}^{a-} > k_{BA(DC)}^{b-}$ and $k_{AB(CD)}^{a+} < k_{AB(CD)}^{b+}$. This leads to $\Gamma_{AB(CD)}^{b+} > \Gamma_{AB(CD)}^{a+}$, when combined with Eq. (7) we obtain. Defining variables \mathcal{X} and \mathcal{Y} as (which would essentially positive in this case),

$$\mathcal{X} = \Gamma_{AB}^{b+} - \Gamma_{AB}^{a+} \quad ; \quad \mathcal{Y} = \Gamma_{CD}^{b+} - \Gamma_{CD}^{a+}, \quad (42)$$

we express

$$\Gamma_{AB}^{ab+} = 2\Gamma_{AB}^{b+} - \mathcal{X} \quad ; \quad \Gamma_{CD}^{ab+} = 2\Gamma_{CD}^{b+} - \mathcal{Y}. \quad (43)$$

Using Eqs. (16), (31), (43), it's straightforward to show that under steady-state conditions, $J_N^b = \frac{1}{2}(\mathcal{X} + \mathcal{Y}) > 0$. Consequently, the spin-polarized particle current is always positive [Dotted red line in FIG. 4(a)].

- If $\kappa < 0$ and $|\kappa| > \varepsilon_L$ i.e. $-\kappa > \varepsilon_L > 0$, the energy eigenstates $|\mathbb{C}\rangle$ and $|\mathbb{D}\rangle$ are swapped [FIG. 1(c)], and Eq. (39) leads to

$$\left(\frac{k_{AB}^{b+} k_{BA}^{a-}}{k_{BA}^{b-} k_{AB}^{a+}} \right) > 1 \quad ; \quad \left(\frac{k_{CD}^{b+} k_{DC}^{a-}}{k_{DC}^{b-} k_{CD}^{a+}} \right) < 1. \quad (44)$$

Using a similar procedure as before, it can be demonstrated that $J_N^b = \frac{1}{2}(\mathcal{X} + \mathcal{Y})$ can take either positive or negative values, depending on the contributions from \mathcal{X} (positive) and \mathcal{Y} (negative), indicating the possibility of the pseudo-ICC [Dashed red line in FIG. 4(a)], given that the conjugate force $\mathcal{F}_N^b = 0$.

In summary, when \mathcal{F}_E^b is the only force acting, J_E^b is always positive [FIG. 4(a)]. If $\kappa > 0$, J_N^b is positive, indicating no ICC. If $-\kappa > \varepsilon_L > 0$, J_N^b can be positive or negative, allowing for pseudo-ICC in the spin-polarized particle current. Equation (40) indicates that both $|\mathbb{A}\rangle \rightarrow |\mathbb{B}\rangle$ and $|\mathbb{C}\rangle \rightarrow |\mathbb{D}\rangle$ transitions are mainly controlled by the bath b , while Eq. (44) suggests a competition between the two baths b and a in controlling the respective transitions, which can make J_N^b negative.

2. Setting \mathcal{F}_E^b as zero: pseudo-ICC in J_E^b

In this case, J_N^b is always positive [FIG. 4(b)], consistent with the non-negativity of the entropy production rate $\dot{\Sigma} = J_N^b \mathcal{F}_N^b$. Since, $\mathcal{F}_E^r = 0$, Eq. (32a) gives

$$\left(\frac{k_{AB}^{a+} k_{BD}^{r+} k_{DC}^{a-} k_{CA}^{r-}}{k_{BA}^{a-} k_{DB}^{r-} k_{CD}^{a+} k_{AC}^{r+}} \right) = 1. \quad (45)$$

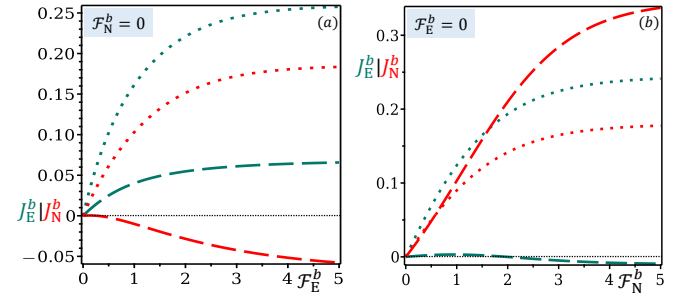


FIG. 4. Variation of the currents J_E^b (bluegreen line) and J_N^b (red line) against the thermodynamic forces (a) \mathcal{F}_E^b while $\mathcal{F}_N^b = 0$ i.e. $(\mu_a \beta = \mu_b \beta_b)$ and (b) \mathcal{F}_N^b while $\mathcal{F}_E^b = 0$ i.e. $(\beta = \beta_b)$. For all cases, the (dashed) dotted lines correspond to $\kappa = (-) + 1.5\hbar\gamma$, validating the condition $|\kappa| > \varepsilon_L$. Other system and bath parameters: $\varepsilon_L = 1.0\hbar\gamma$, $\varepsilon_R = 2.5\hbar\gamma$, $\beta_b = 1/\hbar\gamma$, $\mu_b = 1.0\hbar\gamma$.

We rearrange the above condition as

$$\left(\frac{k_{AB}^{ab+} k_{BD}^{r+} k_{DC}^{ab-} k_{CA}^{r-}}{k_{BA}^{ab-} k_{DB}^{r-} k_{CD}^{ab+} k_{AC}^{r+}} \right) = \left(\frac{k_{AB}^{a-} k_{AB}^{ab+} k_{CD}^{a+} k_{DC}^{ab-}}{k_{AB}^{a+} k_{BA}^{ab-} k_{DC}^{a-} k_{CD}^{ab+}} \right), \quad (46)$$

where the r.h.s is re-written as

$$\text{r.h.s} = \left\{ \frac{1 + (k_{AB}^{b+}/k_{AB}^{a+})}{1 + (k_{BA}^{b-}/k_{BA}^{a-})} \right\} \left\{ \frac{1 + (k_{DC}^{b-}/k_{DC}^{a-})}{1 + (k_{CD}^{b+}/k_{CD}^{a+})} \right\} \equiv \mathcal{P}\mathcal{Q}. \quad (47)$$

It is trivial to show that

$$\begin{aligned} (k_{AB}^{b+}/k_{AB}^{a+}) > 1 \quad \text{and} \quad (k_{BA}^{b-}/k_{BA}^{a-}) < 1 &\Rightarrow \mathcal{P} > 1; \\ (k_{DC}^{b-}/k_{DC}^{a-}) < 1 \quad \text{and} \quad (k_{CD}^{b+}/k_{CD}^{a+}) > 1 &\Rightarrow \mathcal{Q} < 1, \end{aligned} \quad (48)$$

Combining Eqs. (47) and (48), we find that $\mathcal{P}\mathcal{Q} \gtrless 1$. Further, it is possible to verify

$$\left\{ \frac{1 + (k_{AB}^{b+}/k_{AB}^{a+})}{1 + (k_{BA}^{b-}/k_{BA}^{a-})} \right\} < \left\{ \frac{1 + (k_{CD}^{b-}/k_{CD}^{a-})}{1 + (k_{DC}^{b+}/k_{DC}^{a+})} \right\}, \quad (49)$$

under the conditions $\mathcal{F}_E^b \geq 0$ and $\kappa > 0$, which gives $\mathcal{P}\mathcal{Q} < 1$. Thus, r.h.s of Eq. (46) reduces to

$$\left(\frac{k_{AB}^{ab+} k_{BD}^{r+} k_{DC}^{ab-} k_{CA}^{r-}}{k_{BA}^{ab-} k_{DB}^{r-} k_{CD}^{ab+} k_{AC}^{r+}} \right) = \mathcal{P}\mathcal{Q} < 1. \quad (50)$$

For $-\kappa > \varepsilon_L > 0$, similar arguments show that $\mathcal{P}\mathcal{Q} > 1$. As demonstrated in Eqs.(45)-(50), when $\mathcal{F}_E^r = 0$, the value of $\mathcal{P}\mathcal{Q} \leq 1$ for $\mathcal{F}_E^b = 0$ depends on $\kappa \gtrless 0$, considering $|\kappa| > \varepsilon_L$. This leads to:

$$\left(\frac{k_{AB}^{ab+} k_{BD}^{r+} k_{DC}^{ab-} k_{CA}^{r-}}{k_{BA}^{ab-} k_{DB}^{r-} k_{CD}^{ab+} k_{AC}^{r+}} \right) \leq 1. \quad (51)$$

From the steady state condition [Cf. Eq. (16)], Eq. (51) gives

$$\left(\frac{k_{DC}^{ab-} \rho_D}{k_{CD}^{ab+} \rho_C} \right) \leq 1. \quad (52)$$

This implies $\Gamma_{\text{CD}}^{ab+} \gtrless 0$. Substituting into Eq. (43), we find $\Gamma_{\text{CD}}^{b+} \gtrless \frac{\mathcal{Y}}{2}$ for $\kappa \gtrless 0$ and $|\kappa| > \varepsilon_L$, where \mathcal{Y} can be identified as a positive quantity in this case. Thus Γ_{CD}^{b+} is always positive for $\kappa > 0$, making $J_E^b > \kappa \Gamma_{\text{CD}}^{b+}$ always positive [Dotted blue-green line FIG. 4(b)]. For $-\kappa > \varepsilon_L > 0$, $\kappa \Gamma_{\text{CD}}^{b+}$ can be positive or negative, resulting in J_E^b being either positive or negative [Dashed blue-green line FIG. 4(b)].

In summary, with \mathcal{F}_N^b as the only non-zero force, the spin-polarized particle current J_N^b is always positive. The energy current J_E^b is positive for $\kappa > 0$ but can be positive or negative for $-\kappa > \varepsilon_L > 0$. $J_E^b > 0$ reflects cross effect, while $J_E^b < 0$ indicates pseudo-ICC, as the current flows against the non-conjugate particle force \mathcal{F}_N^b . So, true ICC may as well occur in the energy current within this model.

C. Genuine ICC: When both forces are non-zero

From our discussion of the previous two cases, pseudo-ICC occurs in energy and particle currents only for $-\kappa > \varepsilon_L > 0$. Therefore, the search for genuine ICC focuses on the $-\kappa > \varepsilon_L > 0$ ($-1 < \theta < 0$) regime, as pseudo-ICC is a prerequisite for achieving ICC. Thus, w.l.o.g, we limit the analysis to the first quadrant of FIG. 3, where both the forces, $(\mathcal{F}_E^b, \mathcal{F}_N^b)$ are mutually parallel and positive.

1. ICC in particle current J_N^b

Since $(\mathcal{F}_E^b, \mathcal{F}_N^b) > 0$, it readily follows from Eq. (32c)

$$\ln \left(\frac{k_{AB}^{b+} k_{BA}^{a-}}{k_{BA}^{b-} k_{AB}^{a+}} \right) > \left(\frac{\varepsilon_L}{k_B} \right) \mathcal{F}_E^b > 0. \quad (53)$$

Substituting \mathcal{F}_E^b from Eq. (32b) into Eq. (53), we get

$$\ln \left(\frac{k_{AB}^{b+} k_{BA}^{a-}}{k_{BA}^{b-} k_{AB}^{a+}} \right) > \left(\frac{\theta}{1+\theta} \right) \ln \left(\frac{k_{CD}^{b+} k_{DC}^{a-}}{k_{DC}^{b-} k_{CD}^{a+}} \right), \quad (54)$$

which gives

$$\left(\frac{k_{AB}^{b+} k_{BA}^{a-}}{k_{BA}^{b-} k_{AB}^{a+}} \right) > 1; \quad \left(\frac{k_{CD}^{b+} k_{DC}^{a-}}{k_{DC}^{b-} k_{CD}^{a+}} \right) \gtrless 1. \quad (55)$$

The above relations can be classified into two categories:

Case (i): Both arguments are greater than 1. Here, as in Eq. (40), $J_N^b = \frac{1}{2}(\mathcal{X} + \mathcal{Y}) > 0$, since both \mathcal{X} and \mathcal{Y} are positive. This indicates a positive spin-polarized particle current as long as $\mathcal{F}_N^b > 0$.

Case (ii): The latter argument is less than 1, making \mathcal{Y} negative. Following Eq. (44), $J_N^b = \frac{1}{2}(\mathcal{X} + \mathcal{Y}) \gtrless 0$, as \mathcal{X} is positive and \mathcal{Y} is negative. Thus, $J_N^b < 0$ defines genuine ICC [FIG. 5(a)], where the spin-polarized particle current flows against both positive forces \mathcal{F}_N^b and \mathcal{F}_E^b .

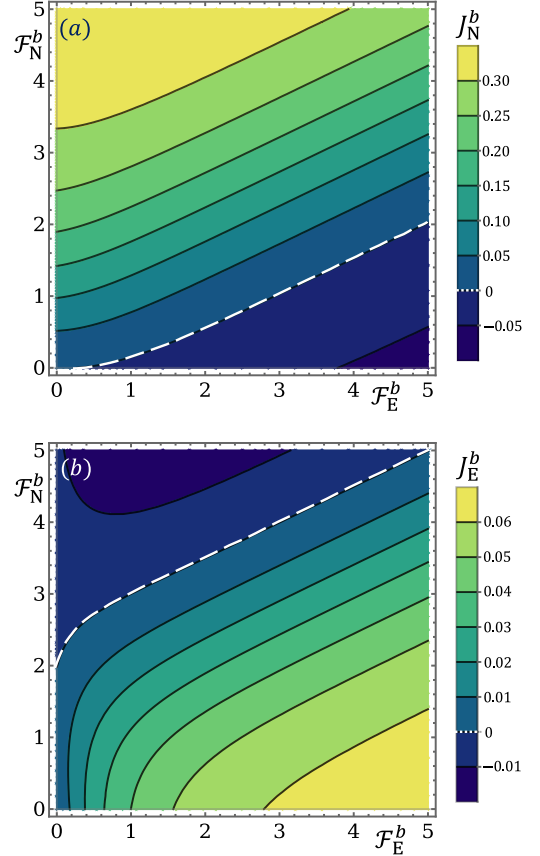


FIG. 5. Variation of (a) the spin-polarised particle current J_N^b and (b) the energy current J_E^b with both the thermodynamic forces for negative κ i.e. $\kappa = -1.5\hbar\gamma$. Genuine ICC for J_N^b occurs in the area below the white dashed line in (a) while it occurs for J_E^b above the white dashed line in (b). Other system and bath parameters: $\varepsilon_L = 1.0\hbar\gamma$, $\varepsilon_R = 2.5\hbar\gamma$, $\beta_b = 1/\hbar\gamma$, $\mu_b = 1.0\hbar\gamma$.

Thus, our reduced three-terminal model can be implemented as the spin-thermoelectric heat engine [19, 21, 58, 59], driving spin-polarized particle flux against the particle force, under the influence of the non-conjugate energy force \mathcal{F}_E^b . The output power is defined as $|(J_N^b \mathcal{F}_N^b / \beta)|$, and the device efficiency is given by

$$\eta = \frac{-J_N^b \cdot \mathcal{F}_N^b}{\beta \cdot J_E^b} = \eta_C - \frac{\dot{\Sigma}}{\beta \cdot J_E^b} \leq \eta_C, \quad (56)$$

where, $\eta_C = (T_{\text{hot}} - T_{\text{cold}})/T_{\text{hot}}$.

2. ICC in energy current J_E^b

When both arguments of Eq. (55) exceed 1, the spin-polarized particle current satisfies $J_N^b > 0$. Consequently, from Eq. (31), $J_E^b > \kappa \Gamma_{\text{CD}}^{b+}$. $\mathcal{F}_E^b = 0$ and $\mathcal{F}_N^b > 0$, under $-\kappa > \varepsilon_L > 0$, it follows from Eq. (45)- (50) that $\mathcal{P}Q > 1$,

leading to

$$\left(\frac{k_{AB}^{ab} + k_{BD}^{r+} k_{DC}^{ab-} k_{CA}^{r-}}{k_{BA}^{ab-} k_{DB}^{r-} k_{CD}^{ab+} k_{AC}^{r+}} \right) > 1. \quad (57)$$

From the established results in Eq. (51), it follows that for the condition $-\kappa > \varepsilon_L > 0$, the following relationships hold: $J_E^b > 0$, $\Gamma_{CD}^{ab+} < 0$, and $\Gamma_{CD}^{b+} < \frac{\mathcal{Y}}{2}$ where $\mathcal{Y} > 0$. Thus, Γ_{CD}^{b+} can be positive or negative, making energy flux $J_E^b > \kappa \Gamma_{CD}^{b+}$, either positive or negative, (i.e., $J_E^b \gtrless 0$). Genuine ICC occurs when $J_E^b < 0$ [FIG. 5(b)], signifying energy flow against positive forces \mathcal{F}_N^b and \mathcal{F}_E^b , simultaneously. Thus, our present model can function as a thermoelectric refrigerator [20, 24, 60–64], driving energy flux against thermal gradient with a COP given by

$$\zeta = \frac{-J_E^b \cdot \beta_b}{J_N^b \cdot \mathcal{F}_N^b} = \zeta_R \left(1 - \frac{\dot{\Sigma}}{J_N^b \cdot \mathcal{F}_N^b} \right) \leq \zeta_R, \quad (58)$$

and bounded by the ideal refrigerator COP.

To summarize, a genuine ICC is achieved in both energy-and spin-polarized particle currents when the two mutually parallel forces \mathcal{F}_E^b and \mathcal{F}_N^b are positive. This allows the model to function as both a spin-thermoelectric heat engine and a refrigerator. The key takeaway from the present model is that the condition $-\kappa > \varepsilon_L > 0$ is essential for observing ICC in energy and particle currents, representing the swapping of energy levels between $|0\uparrow\rangle(|\mathbb{C}\rangle)$ and $|\downarrow\uparrow\rangle(|\mathbb{D}\rangle)$. For, $\kappa > 0$, the eigenstates are arranged in such a way [FIG.1(b)] that the particle (de)excitation implies energy (de)excitation. When $-\kappa > \varepsilon_L > 0$, however, the reordering of the eigenstates [FIG.1(c)] creates an asymmetry between the particle and energy exchange, namely, the particle excitation between $|0\uparrow\rangle \rightarrow |\downarrow\uparrow\rangle$ implies the energetic de-excitation and vice-versa. It is worth mentioning that Wang *et al.* also identified analogous symmetry-breaking as a guiding factor for the emergence of ICC in classical Hamiltonian systems [3]. Thus, it is intuitively evident that some form of symmetry-breaking is necessary to achieve inverse current in coupled quantum transport. In the present model with double QDs, an attractive interdot ($\kappa < 0$) interaction serves as the necessary criterion, while $-\kappa > \varepsilon_L > 0$ acts as the sufficient condition for ICC by breaking the energy-particle exchange symmetry. Furthermore, the present results validate the second law of thermodynamics by ensuring that the two ICC regions do not overlap [FIG. 5]. Specifically, ICC in J_N^b occurs when both arguments of Eq. (55) are positive, whereas for J_E^b , the second argument of Eq. (55) must be negative, in accordance with the sufficient criteria for genuine ICC. Thus, our analysis highlights ICC as a counterintuitive thermodynamic phenomenon distinct from normal cross-effect, and particularly significant for coupled transport

with two mutually parallel thermodynamic forces. Simplifying the three-terminal model (with three force-flux pairs) to a coupled transport system with two parallel forces facilitates the identification of ICC over normal cross-effects, as the three-terminal case, with its complex force directions, makes ICC more challenging to discern.

VIII. CONCLUSION

To conclude, identifying the right thermodynamic forces and their conjugate fluxes in systems with multiple reservoirs is essential for understanding complex thermodynamic phenomena. The present work develops a comprehensive quantum thermodynamic framework for the ICC, where one induced current flows counter to two parallel thermodynamic forces in the system. Using a modified version of the Sánchez-Büttiker model for three-terminal Coulomb-coupled QDs, we investigate the intriguing inverse current behavior in energy and spin-polarized particle currents under near-equilibrium conditions. Our study examines the entropy production rate at both macroscopic and microscopic levels, leveraging the grand-canonical formalism of the Lindblad master equation and Schnakenberg's entropy formulation. The linear structure of the quantum master equation allows for exact analytical expressions for thermodynamic forces and fluxes, incorporating macroscopic reservoir parameters and microscopic system details. This approach uniquely identifies all thermodynamic force-flux pairs for both general and coupled transport systems with mutually parallel forces, enabling a systematic exploration of genuine ICC phenomena in energy and spin-polarized particle currents.

This could open potential applications for unconventional autonomous nano-thermoelectric engines and refrigerators based on the ICC effect in coupled QD systems. Notably, our analysis indicates that an autonomous QD refrigerator or engine requires attractive interactions between QDs as necessary criteria and highlights the possibility for more versatile spin-thermoelectric devices compared to traditional designs, with the novelty rooted in the counter-intuitive thermodynamic behavior of inverse current. A similar concept for an autonomous circular heat engine, inspired by the ICC effect in classical systems [3], has been recently proposed by Benenti *et al.* [65]. We believe our findings will play a crucial role in advancing ICC-assisted unconventional quantum thermoelectric devices in the near future.

ACKNOWLEDGEMENTS

A.G. acknowledges IITK for infrastructure and financial support. S.G. acknowledges the Ministry of Education, Government of India, for the Prime Minister Research Fellowship (PMRF). N.G. is grateful for the FARE fellowship from the institute.

[1] Herbert B. Callen, *Thermodynamics and an Introduction to Thermostatistics*, 2nd ed. (John Wiley & Sons, Inc., New York, 1985).

[2] Dilip Kondepudi and Ilya Prigogine, *Modern Thermodynamics*, 2nd ed. (John Wiley & Sons Ltd, Chichester, 2015).

[3] Jiao Wang, Giulio Casati, and Giuliano Benenti, “Inverse currents in hamiltonian coupled transport,” *Phys. Rev. Lett.* **124**, 110607 (2020).

[4] Yanchao Zhang and Zhenzhen Xie, “Inverse currents in coulomb-coupled quantum dots,” *Phys. Rev. E* **104**, 064142 (2021).

[5] Yanchao Zhang, Shuang Wang, Wanrong Li, and Mingzhuang Yue, “Inverse current induced thermoelectric conversion in a parallel-coupled double quantum dot system,” *Physica Scripta* **98**, 105245 (2023).

[6] Rafael Sánchez and Markus Büttiker, “Optimal energy quanta to current conversion,” *Phys. Rev. B* **83**, 085428 (2011).

[7] Mattia Walschaers, Jorge Fernandez-de-Cossio Diaz, Roberto Mulet, and Andreas Buchleitner, “Optimally designed quantum transport across disordered networks,” *Phys. Rev. Lett.* **111**, 180601 (2013).

[8] Nikolaj Kulvelis, Maxim Dolgushev, and Oliver Mülken, “Universality at breakdown of quantum transport on complex networks,” *Phys. Rev. Lett.* **115**, 120602 (2015).

[9] Juzar Thingna, Daniel Manzano, and Jianshu Cao, “Dynamical signatures of molecular symmetries in nonequilibrium quantum transport,” *Scientific Reports* **6**, 28027 (2016).

[10] Christine Maier, Tiff Brydges, Petar Jurcevic, Nils Trautmann, Cornelius Hempel, Ben P. Lanyon, Philipp Hauke, Rainer Blatt, and Christian F. Roos, “Environment-assisted quantum transport in a 10-qubit network,” *Phys. Rev. Lett.* **122**, 050501 (2019).

[11] Philipp Strasberg, Gernot Schaller, Tobias Brandes, and Massimiliano Esposito, “Thermodynamics of a physical model implementing a maxwell demon,” *Phys. Rev. Lett.* **110**, 040601 (2013).

[12] Aki Kutvonen, Takahiro Sagawa, and Tapio Ala-Nissila, “Thermodynamics of information exchange between two coupled quantum dots,” *Phys. Rev. E* **93**, 032147 (2016).

[13] Krzysztof Ptaszyński and Massimiliano Esposito, “Thermodynamics of quantum information flows,” *Phys. Rev. Lett.* **122**, 150603 (2019).

[14] Björn Annby-Andersson, Peter Samuelsson, Ville F. Maisi, and Patrick P. Potts, “Maxwell’s demon in a double quantum dot with continuous charge detection,” *Phys. Rev. B* **101**, 165404 (2020).

[15] Björn Annby-Andersson, Faraj Bakhshinezhad, Debankur Bhattacharyya, Guilherme De Sousa, Christopher Jarzynski, Peter Samuelsson, and Patrick P. Potts, “Quantum fokker-planck master equation for continuous feedback control,” *Phys. Rev. Lett.* **129**, 050401 (2022).

[16] Björn Annby-Andersson, Debankur Bhattacharyya, Pharnam Bakhshinezhad, Daniel Holst, Guilherme De Sousa, Christopher Jarzynski, Peter Samuelsson, and Patrick P. Potts, “Maxwell’s demon across the quantum-to-classical transition,” *Phys. Rev. Res.* **6**, 043216 (2024).

[17] M. Esposito, K. Lindenberg, and C. Van den Broeck, “Thermoelectric efficiency at maximum power in a quantum dot,” *Europhysics Letters* **85**, 60010 (2009).

[18] Natthapon Nakpathomkun, H. Q. Xu, and Heiner Linke, “Thermoelectric efficiency at maximum power in low-dimensional systems,” *Phys. Rev. B* **82**, 235428 (2010).

[19] S. Donsa, S. Andergassen, and K. Held, “Double quantum dot as a minimal thermoelectric generator,” *Phys. Rev. B* **89**, 125103 (2014).

[20] Yanchao Zhang, Guoxing Lin, and Jincan Chen, “Three-terminal quantum-dot refrigerators,” *Phys. Rev. E* **91**, 052118 (2015).

[21] Holger Thierschmann, Rafael Sánchez, Björn Sothmann, Fabian Arnold, Christian Heyn, Wolfgang Hansen, Hartmut Buhmann, and Laurens W. Molenkamp, “Three-terminal energy harvester with coupled quantum dots,” *Nature Nanotechnology* **10**, 854–858 (2015).

[22] Robert S. Whitney, Rafael Sánchez, Federica Haupt, and Janine Splettstoesser, “Thermoelectricity without absorbing energy from the heat sources,” *Physica E: Low-dimensional Systems and Nanostructures* **75**, 257–265 (2016).

[23] Paolo Andrea Erdman, Francesco Mazza, Riccardo Bosio, Giuliano Benenti, Rosario Fazio, and Fabio Taddei, “Thermoelectric properties of an interacting quantum dot based heat engine,” *Phys. Rev. B* **95**, 245432 (2017).

[24] Paolo Andrea Erdman, Bibek Bhandari, Rosario Fazio, Jukka P. Pekola, and Fabio Taddei, “Absorption refrigerators based on coulomb-coupled single-electron systems,” *Phys. Rev. B* **98**, 045433 (2018).

[25] Robert S. Whitney, Rafael Sánchez, and Janine Splettstoesser, “Quantum thermodynamics of nanoscale thermoelectrics and electronic devices,” in *Thermodynamics in the Quantum Regime: Fundamental Aspects and New Directions*, edited by Felix Binder, Luis A. Correa, Christian Gogolin, Janet Anders, and Gerardo Adesso (Springer International Publishing, Cham, 2018) pp. 175–206.

[26] Gonzalo Manzano, Rafael Sánchez, Ralph Silva, Géraldine Haack, Jonatan B. Brask, Nicolas Brunner, and Patrick P. Potts, “Hybrid thermal machines: Generalized thermodynamic resources for multitasking,” *Phys. Rev. Res.* **2**, 043302 (2020).

[27] Luqin Wang, Zi Wang, Chen Wang, and Jie Ren, “Cycle flux ranking of network analysis in quantum thermal devices,” *Phys. Rev. Lett.* **128**, 067701 (2022).

[28] Nikhil Gupt, Shuvadip Ghosh, and Arnab Ghosh, “Graph theoretic analysis of three-terminal quantum dot thermocouples: Onsager relations and spin-thermoelectric effects,” *Phys. Rev. B* **109**, 125124 (2024).

[29] Tomi Ruokola and Teemu Ojanen, “Single-electron heat diode: Asymmetric heat transport between electronic reservoirs through coulomb islands,” *Phys. Rev. B* **83**, 241404 (2011).

[30] T. Werlang, M. A. Marchiori, M. F. Cornelio, and D. Valente, “Optimal rectification in the ultrastrong coupling regime,” *Phys. Rev. E* **89**, 062109 (2014).

[31] Yanchao Zhang, Xin Zhang, Zhuolin Ye, Guoxing Lin, and Jincan Chen, “Three-terminal quantum-dot thermal management devices,” *Applied Physics Letters* **110**, 153501 (2017).

[32] A. A. Aligia, D. Pérez Daroca, Liliana Arrachea, and P. Roura-Bas, “Heat current across a capacitively coupled double quantum dot,” *Phys. Rev. B* **101**, 075417 (2020).

[33] Ludovico Tesser, Bibek Bhandari, Paolo Andrea Erdman, Elisabetta Paladino, Rosario Fazio, and Fabio Taddei, “Heat rectification through single and coupled quantum dots,” *New Journal of Physics* **24**, 035001 (2022).

[34] Shuvadip Ghosh, Nikhil Gupt, and Arnab Ghosh, “Universal behavior of the coulomb-coupled fermionic thermal diode,” *Entropy* **24** (2022).

[35] Massimiliano Esposito, Niraj Kumar, Katja Lindenberg, and Christian Van den Broeck, “Stochastically driven single-level quantum dot: A nanoscale finite-time thermodynamic machine and its various operational modes,” *Phys. Rev. E* **85**, 031117 (2012).

[36] Jian-Hua Jiang, Manas Kulkarni, Dvira Segal, and Yoseph Imry, “Phonon thermoelectric transistors and rectifiers,” *Phys. Rev. B* **92**, 045309 (2015).

[37] Jing Yang, Cyril Elouard, Janine Splettstoesser, Björn Sothmann, Rafael Sánchez, and Andrew N. Jordan, “Thermal transistor and thermometer based on coulomb-coupled conductors,” *Phys. Rev. B* **100**, 045418 (2019).

[38] B. Dutta, J. T. Peltonen, D. S. Antonenko, M. Meschke, M. A. Skvortsov, B. Kubala, J. König, C. B. Winkelmann, H. Courtois, and J. P. Pekola, “Thermal conductance of a single-electron transistor,” *Phys. Rev. Lett.* **119**, 077701 (2017).

[39] B. Dutta, D. Majidi, N. W. Talarico, N. Lo Gullo, H. Courtois, and C. B. Winkelmann, “Single-quantum-dot heat valve,” *Phys. Rev. Lett.* **125**, 237701 (2020).

[40] Yanchao Zhang, Zhimin Yang, Xin Zhang, Bihong Lin, Guoxing Lin, and Jincan Chen, “Coulomb-coupled quantum-dot thermal transistors,” *EPL (Europhysics Letters)* **122**, 17002 (2018).

[41] Upendra Harbola, Massimiliano Esposito, and Shaul Mukamel, “Quantum master equation for electron transport through quantum dots and single molecules,” *Phys. Rev. B* **74**, 235309 (2006).

[42] Sudarson Sekhar Sinha, Arnab Ghosh, and Deb Shankar Ray, “Quantum smoluchowski equation for a spin bath,” *Phys. Rev. E* **84**, 031118 (2011).

[43] Sudarson Sekhar Sinha, Arnab Ghosh, and Deb Shankar Ray, “Decay of a metastable state induced by a spin bath,” *Phys. Rev. E* **84**, 041113 (2011).

[44] Arnab Ghosh, Sudarson Sekhar Sinha, and Deb Shankar Ray, “Fermionic oscillator in a fermionic bath,” *Phys. Rev. E* **86**, 011138 (2012).

[45] Mukul Agrawal and G. S. Solomon, “Quantum-well band structure effects on the emission polarization from a spin-polarized electron reservoir,” *Applied Physics Letters* **85**, 1820–1822 (2004).

[46] Koen Vandaele, Sarah J. Watzman, Benedetta Flebus, Arati Prakash, Yuanhua Zheng, Stephen R. Boona, and Joseph P. Heremans, “Thermal spin transport and energy conversion,” *Materials Today Physics* **1**, 39–49 (2017).

[47] Nikhil Gupt, Srijan Bhattacharyya, and Arnab Ghosh, “Statistical generalization of regenerative bosonic and fermionic stirling cycles,” *Phys. Rev. E* **104**, 054130 (2021).

[48] D. Perez Daroca, P. Roura-Bas, and A. A. Aligia, “Role of asymmetry in thermoelectric properties of a double quantum dot out of equilibrium,” *Phys. Rev. B* **111**, 045134 (2025).

[49] I. H. Chan, R. M. Westervelt, K. D. Maranowski, and A. C. Gossard, “Strongly capacitively coupled quantum dots,” *Applied Physics Letters* **80**, 1818–1820 (2002).

[50] B. Dutta, D. Majidi, N. W. Talarico, N. Lo Gullo, H. Courtois, and C. B. Winkelmann, “Single-quantum-dot heat valve,” *Phys. Rev. Lett.* **125**, 237701 (2020).

[51] Nikhil Gupt, Shuvadip Ghosh, and Arnab Ghosh, “Top-ranked cycle flux network analysis of molecular photo-cells,” *Phys. Rev. E* **108**, 034305 (2023).

[52] Heinz-Peter Breuer and Francesco Petruccione, *The Theory of Open Quantum Systems* (Oxford University Press, 2007).

[53] Philipp Strasberg, *Quantum Stochastic Thermodynamics: Foundations and Selected Applications* (Oxford University Press, 2022).

[54] J. Schnakenberg, “Network theory of microscopic and macroscopic behavior of master equation systems,” *Rev. Mod. Phys.* **48**, 571–585 (1976).

[55] Massimiliano Esposito, Katja Lindenberg, and Christian Van den Broeck, “Entropy production as correlation between system and reservoir,” *New Journal of Physics* **12**, 013013 (2010).

[56] Gabriel T. Landi and Mauro Paternostro, “Irreversible entropy production: From classical to quantum,” *Rev. Mod. Phys.* **93**, 035008 (2021).

[57] Ronnie Kosloff, “Quantum thermodynamics: A dynamical viewpoint,” *Entropy* **15**, 2100–2128 (2013).

[58] A.-M. Daré and P. Lombardo, “Powerful coulomb-drag thermoelectric engine,” *Phys. Rev. B* **96**, 115414 (2017).

[59] Aniket Singha, “A realistic non-local heat engine based on Coulomb-coupled systems,” *Journal of Applied Physics* **127**, 234903 (2020).

[60] A.-M. Daré, “Comparative study of heat-driven and power-driven refrigerators with coulomb-coupled quantum dots,” *Phys. Rev. B* **100**, 195427 (2019).

[61] Swarnadip Mukherjee, Bitan De, and Bhaskaran Muralidharan, “Three-terminal vibron-coupled hybrid quantum dot thermoelectric refrigeration,” *Journal of Applied Physics* **128**, 234303 (2020).

[62] R. David Mayrhofer, Cyril Elouard, Janine Splettstoesser, and Andrew N. Jordan, “Stochastic thermodynamic cycles of a mesoscopic thermoelectric engine,” *Phys. Rev. B* **103**, 075404 (2021).

[63] Anamika Barman, Surojit Halder, Shailendra K. Varshney, Gourab Dutta, and Aniket Singha, “Realistic non-local refrigeration engine based on coulomb-coupled systems,” *Phys. Rev. E* **103**, 012131 (2021).

[64] Mohammed Ali Aamir, Paul Jamet Suria, José Antonio Marín Guzmán, Claudia Castillo-Moreno, Jeffrey M. Epstein, Nicole Yunger Halpern, and Simone Gasparinetti, “Thermally driven quantum refrigerator autonomously resets a superconducting qubit,” (2025).

[65] Giuliano Benenti, Giulio Casati, Fabio Marchesoni, and Jiao Wang, “Autonomous circular heat engine,” *Phys. Rev. E* **106**, 044104 (2022).

[66] Nikhil Gupt, Srijan Bhattacharyya, Bikash Das, Subhadeep Datta, Victor Mukherjee, and Arnab Ghosh, “Floquet quantum thermal transistor,” *Phys. Rev. E* **106**, 024110 (2022).

Appendix A: Derivation of the Lindblad Master Equation

We present the interaction picture master equation to study the system's dynamical evolution that exchanges particles and energy with the reservoirs. Let us start with the tunneling Hamiltonian

$$H_T = \sum_{\alpha\lambda} H_T^{\alpha\lambda} = \sum_{\alpha\lambda} \sum_k \hbar [t_k^{\alpha\lambda} c_{\lambda k}^\dagger d_\alpha + t_k^{\alpha\lambda*} d_\alpha^\dagger c_{\lambda k}] \quad (\text{A1})$$

To derive the master equation, we start with the von Neumann equation for the total density matrix ρ_{tot} in the interaction picture

$$\frac{d}{dt} \rho_{\text{tot}} = -\frac{i}{\hbar} [H_T(t), \rho_{\text{tot}}(t)]. \quad (\text{A2})$$

Integrating the above equation, and taking a trace over the bath degrees of freedom, one obtains

$$\frac{\partial}{\partial t} \rho_s(t) = \frac{1}{(i\hbar)^2} \int_0^t dt' \text{Tr}_\lambda [H_T(t), [H_T(t-t'), \rho_{\text{tot}}(t')]], \quad (\text{A3})$$

where Tr_λ refers to the trace over each bath degrees of freedom and $\text{Tr}_\lambda\{\rho_{\text{tot}}(t)\} = \rho_s(t)$ denotes the reduced density operator for the system. We also assume that $\text{Tr}_\lambda[H_T(t), \rho_{\text{tot}}(0)] = 0$. Under the Born-Markov approximation, the above equation can be rewritten as [34, 52, 66]

$$\dot{\rho}_s(t) = \frac{1}{(i\hbar)^2} \sum_\lambda \int_0^\infty dt' \text{Tr}_\lambda [H_T^\lambda(t), [H_T^\lambda(t-t'), \rho_s(t) \otimes \rho_a \otimes \rho_b \otimes \rho_r]], \quad (\text{A4})$$

where we use the following properties of the bath operators $\text{Tr}_\lambda\{c_\lambda(t)\rho_\lambda\} = 0 = \text{Tr}_\lambda\{c_\lambda^\dagger(t)\rho_\lambda\}$ and $\text{Tr}_\lambda\{[H_T^\lambda(t), [H_T^\lambda(t-t'), \rho_s(t) \otimes \rho_a \otimes \rho_b \otimes \rho_r]]\} = 0; \lambda \neq \nu; \lambda, \nu = a, b, r$. Now, in the above equation, we use the interaction picture system and bath operators

$$\begin{aligned} d_\alpha(t) &= e^{iH_s t/\hbar} d_\alpha e^{-iH_s t/\hbar} = \sum_{\omega_{ij} > 0} e^{-i\omega_{ij} t/\hbar} d_\alpha; & \alpha &= L, R \\ c_\lambda(t) &= e^{iH_B t/\hbar} c_\lambda e^{-iH_B t/\hbar} = \sum_k e^{-i(\epsilon_k^\lambda - \mu_\lambda)t/\hbar} c_\lambda; \end{aligned} \quad (\text{A5})$$

and their hermitian adjoints, where ω_{ij} is defined as the transition energy for the transition between the system eigenstates $|i\rangle$ and $|j\rangle$. Eliminating the high-frequency oscillating terms by the standard procedure of secular approximation, one can finally derive the master equation in the following form

$$\dot{\rho}_s(t) = \sum_\lambda \mathcal{L}_\lambda[\rho_s(t)], \quad (\text{A6})$$

where the Lindblad operators $\mathcal{L}_\lambda[\rho_s(t)]$ are given by

$$\begin{aligned} \mathcal{L}_\lambda[\rho_s(t)] &= \sum_{\{\omega_\alpha\} > 0} \mathcal{G}_\lambda(\omega_\alpha) \left[d_\alpha^\dagger(\omega_\alpha) \rho_s d_\alpha(\omega_\alpha) - \frac{1}{2} \{ \rho_s, d_\alpha(\omega_\alpha) d_\alpha^\dagger(\omega_\alpha) \} \right] \\ &\quad + \mathcal{G}_\lambda(-\omega_\alpha) \left[d_\alpha(\omega_\alpha) \rho_s d_\alpha^\dagger(\omega_\alpha) - \frac{1}{2} \{ \rho_s, d_\alpha^\dagger(\omega_\alpha) d_\alpha(\omega_\alpha) \} \right]. \end{aligned} \quad (\text{A7})$$

In the above equation, we define the temperature-dependent bath spectral functions as

$$\mathcal{G}_\lambda(\omega_\alpha) = \gamma_\lambda(\omega_\alpha) f_\lambda^+(\omega_\alpha); \quad \mathcal{G}_\lambda(-\omega_\alpha) = \gamma_\lambda(\omega_\alpha) f_\lambda^-(\omega_\alpha), \quad (\text{A8})$$

where $\gamma_\lambda(\omega_\alpha)$ is the bare electron transfer rate between the reservoir λ and coupled QD $_\alpha$. The explicit forms in terms of the system-reservoir coupling constants can be calculated using Fermi's golden rule, as $\gamma_\lambda(\omega_\alpha) \equiv \gamma_\lambda(\omega_\alpha) = 2\pi \sum_k |t_k^{\alpha\lambda}|^2 \delta(\omega_\alpha - \epsilon_k^\lambda)$, where ω_α represents the required amount of energy associated with the transition between QD $_\alpha$ and its coupled lead. The function $f_\lambda^\pm(\omega_{ij})$ represents the Fermi distribution functions (FDF) which are obtained by

tracing over the bath density operator, for example, $f_{\lambda}^+(\omega_{ij}) = \text{Tr}_{\lambda}(c_{\lambda}^{\dagger} c_{\lambda} \rho_{\lambda})$, and $f_{\lambda}^-(\omega_{ij}) = \text{Tr}_{\lambda}(c_{\lambda} c_{\lambda}^{\dagger} \rho_{\lambda})$, where the bath operators c_{λ}^{\dagger} and c_{λ} obey anti-commutation relation and the reservoir governs the transition between eigenstate $|i\rangle$ to $|j\rangle$, that costs ω_{ij} amount of energy. The explicit expressions of the FDFs for various transitions are mentioned in the main text.

Now to derive the forms of the Lindbladians, we need to express the creation and the annihilation operators in terms of the system eigenstates in the following forms,

$$\begin{aligned} \sum_{\{\omega_L\}} d_L^{\dagger}(\omega_L) &= d_L^{\dagger}(\omega_{AB}) + d_L^{\dagger}(\omega_{CD}) = |\mathbb{B}\rangle\langle\mathbb{A}| + |\mathbb{D}\rangle\langle\mathbb{C}| \\ \sum_{\{\omega_R\}} d_R^{\dagger}(\omega_R) &= d_R^{\dagger}(\omega_{AC}) + d_R^{\dagger}(\omega_{BD}) = |\mathbb{C}\rangle\langle\mathbb{A}| + |\mathbb{D}\rangle\langle\mathbb{B}| \\ \sum_{\{\omega_L\}} d_L(\omega_L) &= d_L(\omega_{BA}) + d_L(\omega_{DC}) = |\mathbb{A}\rangle\langle\mathbb{B}| + |\mathbb{C}\rangle\langle\mathbb{D}| \\ \sum_{\{\omega_R\}} d_R(\omega_R) &= d_R(\omega_{CA}) + d_R(\omega_{DB}) = |\mathbb{A}\rangle\langle\mathbb{C}| + |\mathbb{B}\rangle\langle\mathbb{D}| \end{aligned} \quad (A9)$$

So, the time evolution of the occupation probabilities which are essentially the diagonal elements of the reduced density matrix $\rho_{ii} = \langle i|\rho_s(t)|i\rangle$, can be obtained using the LME [Eq. (A8)] as follows,

$$\dot{\rho}_{ii} \equiv \frac{d\rho_{ii}}{dt} = \langle i|\dot{\rho}_s(t)|i\rangle = \sum_{\lambda} \langle i|\mathcal{L}_{\lambda}[\rho_s(t)]|i\rangle. \quad (A10)$$

Appendix B: Explicit expressions of various currents

From Eq. (15), one can evaluate the explicit expressions of both energy and particle currents for each reservoir in the following way

$$\begin{aligned} J_E^a &= \omega_{AB}\Gamma_{AB}^{a+} + \omega_{CD}\Gamma_{CD}^{a+} = \varepsilon_L\Gamma_{AB}^{a+} + (\varepsilon_L + \kappa)\Gamma_{CD}^{a+}; & J_E^b &= \omega_{AB}\Gamma_{AB}^{b+} + \omega_{CD}\Gamma_{CD}^{b+} = \varepsilon_L\Gamma_{AB}^{b+} + (\varepsilon_L + \kappa)\Gamma_{CD}^{b+}; \\ J_E^r &= \omega_{AC}\Gamma_{AC}^{r+} + \omega_{BD}\Gamma_{BD}^{r+} = \varepsilon_R\Gamma_{AC}^{r+} + (\varepsilon_R + \kappa)\Gamma_{BD}^{r+}; & J_N^a &= \Gamma_{AB}^{a+} + \Gamma_{CD}^{a+}; & J_N^b &= \Gamma_{AB}^{b+} + \Gamma_{CD}^{b+}; & J_N^r &= \Gamma_{AC}^{r+} + \Gamma_{BD}^{r+}. \end{aligned} \quad (B1)$$

Inserting the above relations, the expression of the heat current associated with each reservoir can be evaluated as

$$J_Q^a = (\varepsilon_L - \mu_a)\Gamma_{AB}^{a+} + (\varepsilon_L + \kappa - \mu_a)\Gamma_{CD}^{a+}; \quad J_Q^b = (\varepsilon_L - \mu_b)\Gamma_{AB}^{b+} + (\varepsilon_L + \kappa - \mu_b)\Gamma_{CD}^{b+}; \quad J_Q^r = (\varepsilon_R - \mu_r)\Gamma_{AC}^{r+} + (\varepsilon_R + \kappa - \mu_r)\Gamma_{BD}^{r+}. \quad (B2)$$

Appendix C: Expression of the steady state transition rate

To determine the steady-state transition rate, we rewrite Eq. (6)-(8) as

$$\mathcal{M} \begin{bmatrix} \rho_A \\ \rho_B \\ \rho_C \\ \rho_D \end{bmatrix} = \begin{bmatrix} 0 \\ 0 \\ 0 \\ 1 \end{bmatrix}, \quad (C1)$$

subject to the condition $\rho_A + \rho_B + \rho_C + \rho_D = 1$, and

$$\mathcal{M} = \begin{bmatrix} -f_r^{1+} - f_a^{1+} - f_b^{1+} & f_a^{1-} + f_b^{1-} & f_r^{1+} & 0 \\ f_a^{1+} + f_b^{1+} & -f_a^{1-} - f_b^{1-} - f_r^{2+} & 0 & f_r^{2-} \\ f_r^{1+} & 0 & -f_a^{2+} - f_b^{2+} - f_r^{1-} & f_a^{2-} + f_b^{2-} \\ 1 & 1 & 1 & 1 \end{bmatrix}, \quad (C2)$$

where, for the sake of simplicity of our analysis, we assume that $\gamma_a \simeq \gamma_b \simeq \gamma_r \equiv \gamma$. Solving Eq. (C1) with the above matrix \mathcal{M} , one can obtain the steady state population $\{\rho_i\}$ in terms of which we can evaluate the explicit expression

$$\Gamma_{\circlearrowleft} = -\Gamma_{\circlearrowright} = \gamma \left[\frac{f_{ab}^{1+}[f_{ab}^{2+}(f_r^{2+} - f_r^{1+}) + 2f_r^{2+}(f_r^{1+} - 1)] - 2f_r^{1+}f_{ab}^{2+}(f_r^{2+} - 1)}{3f_{ab}^{1+}(f_r^{1+} - f_r^{2+}) - 6 + 3f_{ab}^{2+}(f_r^{2+} - f_r^{1+})} \right], \quad (C3)$$

where, we define $f_{ab}^{1+(2+)} = f_a^{1+(2+)} + f_b^{1+(2+)}$.

Appendix D: Non-negativity of entropy production rate

One can evaluate the expression of the entropy production (Σ) from the entropy change of the system ($\Delta\mathcal{S}_s = \mathcal{S}_s(t) - \mathcal{S}_s(0)$), which is defined as

$$\Delta\mathcal{S}_s(t) = -k_B \text{Tr}_s[\rho_s(t) \ln \rho_s(t)] + k_B \text{Tr}_s[\rho_s(0) \ln \rho_s(0)] = -k_B \text{Tr}[\rho_{\text{tot}}(t) \ln \rho_s(t)] + k_B \text{Tr}[\rho_{\text{tot}}(0) \ln \rho_s(0)]. \quad (\text{D1})$$

We assume that the initial equilibrium state, $\rho_{\text{tot}}(0)$ does not display any entanglement or correlation between the system and the environment. Therefore

$$\rho_{\text{tot}}(0) = \rho_s(0) \prod_{\lambda} \rho_{\lambda}^{\text{eq}}. \quad (\text{D2})$$

Inserting Eq. (D2) into Eq. (D1), we can continue as follows

$$\begin{aligned} \Delta\mathcal{S}_s(t) &= -k_B \text{Tr}[\rho_{\text{tot}}(t) \ln \rho_s(t)] + k_B \text{Tr}[\rho_{\text{tot}}(0) \ln \rho_{\text{tot}}(0)] - k_B \sum_{\lambda} \text{Tr}[\rho_{\text{tot}}(0) \ln \rho_{\lambda}^{\text{eq}}] \\ &= -k_B \text{Tr} \left[\rho_{\text{tot}}(t) \ln \left\{ \rho_s(t) \prod_{\lambda} \rho_{\lambda}^{\text{eq}} \right\} \right] + k_B \text{Tr}[\rho_{\text{tot}}(0) \ln \rho_{\text{tot}}(0)] + k_B \sum_{\lambda} \text{Tr}_{\lambda}[\{\rho_{\lambda}(t) - \rho_{\lambda}^{\text{eq}}\} \ln \rho_{\lambda}^{\text{eq}}]. \end{aligned} \quad (\text{D3})$$

Again, $\rho_{\text{tot}}(t)$ and $\rho_{\text{tot}}(0)$ are related through unitary evolution $\rho_{\text{tot}}(t) = \mathcal{U}\rho_{\text{tot}}(0)\mathcal{U}^{\dagger}$, which implies $\text{Tr}[\rho_{\text{tot}}(t) \ln \rho_{\text{tot}}(t)] = \text{Tr}[\rho_{\text{tot}}(0) \ln \rho_{\text{tot}}(0)]$. Applying this relation in the above equation, the final expression of the entropy change of the system can be calculated as

$$\Delta\mathcal{S}_s(t) = -k_B \text{Tr} \left[\rho_{\text{tot}}(t) \ln \left\{ \rho_s(t) \prod_{\lambda} \rho_{\lambda}^{\text{eq}} \right\} \right] + k_B \text{Tr}[\rho_{\text{tot}}(t) \ln \rho_{\text{tot}}(t)] + k_B \sum_{\lambda} \text{Tr}_{\lambda}[\{\rho_{\lambda}(t) - \rho_{\lambda}^{\text{eq}}\} \ln \rho_{\lambda}^{\text{eq}}]. \quad (\text{D4})$$

The last term of the above equation can be identified as the *entropy flow* (Φ), representing the reversible contribution to the system entropy change due to heat exchange with the reservoirs. A comparison of the above equation with Eq. (19), defines the *entropy production*, representing the irreversible contribution to the entropy change of the system and the *entropy flow* as

$$\Sigma(t) = k_B \text{Tr}[\rho_{\text{tot}}(t) \ln \{\rho_{\text{tot}}(t)\}] - k_B \text{Tr} \left[\rho_{\text{tot}}(t) \ln \left\{ \rho_s(t) \prod_{\lambda} \rho_{\lambda}^{\text{eq}} \right\} \right]; \quad \Phi(t) = k_B \sum_{\lambda} \text{Tr}_{\lambda}[\{\rho_{\lambda}(t) - \rho_{\lambda}^{\text{eq}}\} \ln \rho_{\lambda}^{\text{eq}}]. \quad (\text{D5})$$

The above expression of the *entropy production* can be expressed in terms of the relative entropy

$$\Sigma(t) \equiv \mathcal{D} \left[\rho_{\text{tot}}(t) \parallel \left\{ \rho_s(t) \prod_{\lambda} \rho_{\lambda}^{\text{eq}} \right\} \right], \quad (\text{D6})$$

where $\mathcal{D}[\rho \parallel \rho']$ is the quantum relative entropy between two density matrices ρ and ρ' , defined via

$$\mathcal{D}[\rho \parallel \rho'] := \text{Tr}[\rho \ln \rho] - \text{Tr}[\rho \ln \rho']. \quad (\text{D7})$$

The non-negativity of relative entropy is affirmed, attaining a value of zero solely in the case of complete matrix identity. While the non-negativity of entropy production doesn't imply the same for its rate, in the limit of large reservoirs, $\Sigma(t)$ is expected to converge to a convex, monotonically increasing function of time [55]. In the same limit, if the system dynamics are described by a Markovian quantum Lindblad master equation, implying entropy production as a convex functional of the system density matrix [52, 55], the entropy production rate $\dot{\Sigma}(t)$ would eventually be positive, only reaching zero for the equilibrium state.

Appendix E: Derivation of the microscopic definition of the entropy production rate

Considering the von Neumann entropy defined as $\mathcal{S}_s(t) = -k_B \sum_{\mathbb{A}} \rho_{\mathbb{A}}(t) \ln \rho_{\mathbb{A}}(t)$, where, $\rho_{\mathbb{A}}$ signifies populations of the system eigenstates ($\mathbb{A} = \mathbb{A}, \mathbb{B}, \mathbb{C}, \mathbb{D}$), the change in the system entropy is given by

$$\Delta\mathcal{S}_s(t) = \mathcal{S}_s(t) - \mathcal{S}_s(0) = -k_B \sum_{\mathbb{A}} \rho_{\mathbb{A}}(t) \ln \rho_{\mathbb{A}}(t) + k_B \sum_{\mathbb{A}} \rho_{\mathbb{A}}(0) \ln \rho_{\mathbb{A}}(0). \quad (\text{E1})$$

So, the time evolution of the entropy change can be evaluated as

$$\frac{d}{dt} \Delta S_s(t) = -k_B \sum_i \dot{\rho}_i(t) \ln \rho_i(t) + k_B \sum_i \dot{\rho}_i(0) \ln \rho_i(0) = -k_B \sum_i \dot{\rho}_i(t) \ln \rho_i(t) \equiv -k_B \sum_i \dot{\rho}_i \ln \rho_i. \quad (\text{E2})$$

Now, using Eq. (6) for $\dot{\rho}_i$, we recover Eq. (28) of the main text:

$$\frac{d}{dt} \Delta S_s(t) = k_B \left[\Gamma_{AB}^{a+} \ln \left(\frac{\rho_A}{\rho_B} \right) + \Gamma_{AB}^{b+} \ln \left(\frac{\rho_A}{\rho_B} \right) + \Gamma_{BD}^{r+} \ln \left(\frac{\rho_B}{\rho_D} \right) + \Gamma_{DC}^{a-} \ln \left(\frac{\rho_D}{\rho_C} \right) + \Gamma_{DC}^{b-} \ln \left(\frac{\rho_D}{\rho_C} \right) + \Gamma_{CA}^{r-} \ln \left(\frac{\rho_C}{\rho_A} \right) \right]. \quad (\text{E3})$$

By comparing the above equation with Eq. (19), we obtain Eq. (29) for the general expressions of $\dot{\Sigma}(t)$ and $\dot{\Phi}(t)$:

$$\begin{aligned} \dot{\Sigma}(t) &= k_B \left[\Gamma_{AB}^{a+} \ln \left(\frac{k_{AB}^{a+} \rho_A}{k_{BA}^{a-} \rho_B} \right) + \Gamma_{AB}^{b+} \ln \left(\frac{k_{AB}^{b+} \rho_A}{k_{BA}^{b-} \rho_B} \right) + \Gamma_{BD}^{r+} \ln \left(\frac{k_{BD}^{r+} \rho_B}{k_{DB}^{r-} \rho_D} \right) + \Gamma_{DC}^{a-} \ln \left(\frac{k_{DC}^{a-} \rho_D}{k_{CD}^{a+} \rho_C} \right) + \Gamma_{DC}^{b-} \ln \left(\frac{k_{DC}^{b-} \rho_D}{k_{CD}^{b+} \rho_C} \right) + \Gamma_{CA}^{r-} \ln \left(\frac{k_{CA}^{r-} \rho_C}{k_{AC}^{r+} \rho_A} \right) \right] \\ &= k_B \left[(k_{AB}^{a+} \rho_A - k_{BA}^{a-} \rho_B) \ln \left(\frac{k_{AB}^{a+} \rho_A}{k_{BA}^{a-} \rho_B} \right) + (k_{AB}^{b+} \rho_A - k_{BA}^{b-} \rho_B) \ln \left(\frac{k_{AB}^{b+} \rho_A}{k_{BA}^{b-} \rho_B} \right) + (k_{BD}^{r+} \rho_B - k_{DB}^{r-} \rho_D) \ln \left(\frac{k_{BD}^{r+} \rho_B}{k_{DB}^{r-} \rho_D} \right) \right. \\ &\quad \left. + (k_{DC}^{a-} \rho_D - k_{CD}^{a+} \rho_C) \ln \left(\frac{k_{DC}^{a-} \rho_D}{k_{CD}^{a+} \rho_C} \right) + (k_{DC}^{b-} \rho_D - k_{CD}^{b+} \rho_C) \ln \left(\frac{k_{DC}^{b-} \rho_D}{k_{CD}^{b+} \rho_C} \right) + (k_{CA}^{r-} \rho_C - k_{AC}^{r+} \rho_A) \ln \left(\frac{k_{CA}^{r-} \rho_C}{k_{AC}^{r+} \rho_A} \right) \right], \\ \dot{\Phi}(t) &= -k_B \left[\Gamma_{AB}^{a+} \ln \left(\frac{k_{AB}^{a+}}{k_{BA}^{a-}} \right) + \Gamma_{AB}^{b+} \ln \left(\frac{k_{AB}^{b+}}{k_{BA}^{b-}} \right) + \Gamma_{BD}^{r+} \ln \left(\frac{k_{BD}^{r+}}{k_{DB}^{r-}} \right) + \Gamma_{DC}^{a-} \ln \left(\frac{k_{DC}^{a-}}{k_{CD}^{a+}} \right) + \Gamma_{DC}^{b-} \ln \left(\frac{k_{DC}^{b-}}{k_{CD}^{b+}} \right) + \Gamma_{CA}^{r-} \ln \left(\frac{k_{CA}^{r-}}{k_{AC}^{r+}} \right) \right]. \end{aligned} \quad (\text{E4})$$

There is no net entropy change in the system at the steady state, which reduces Eq. (30) for the form of the entropy production rate:

$$\begin{aligned} \dot{\Sigma}(t) &= -\dot{\Phi}(t) = k_B \left[\Gamma_{AB}^{a+} \ln \left(\frac{k_{AB}^{a+}}{k_{BA}^{a-}} \right) + \Gamma_{AB}^{b+} \ln \left(\frac{k_{AB}^{b+}}{k_{BA}^{b-}} \right) + \Gamma_{BD}^{r+} \ln \left(\frac{k_{BD}^{r+}}{k_{DB}^{r-}} \right) + \Gamma_{DC}^{a-} \ln \left(\frac{k_{DC}^{a-}}{k_{CD}^{a+}} \right) + \Gamma_{DC}^{b-} \ln \left(\frac{k_{DC}^{b-}}{k_{CD}^{b+}} \right) + \Gamma_{CA}^{r-} \ln \left(\frac{k_{CA}^{r-}}{k_{AC}^{r+}} \right) \right] \\ &= k_B \left[\Gamma_{AB}^{ab+} \ln \left(\frac{k_{AB}^{a+}}{k_{BA}^{a-}} \right) + \Gamma_{BD}^{r+} \ln \left(\frac{k_{BD}^{r+}}{k_{DB}^{r-}} \right) + \Gamma_{DC}^{ab-} \ln \left(\frac{k_{DC}^{a-}}{k_{CD}^{a+}} \right) + \Gamma_{CA}^{r-} \ln \left(\frac{k_{CA}^{r-}}{k_{AC}^{r+}} \right) \right] + k_B \left[\Gamma_{AB}^{b+} \ln \left(\frac{k_{AB}^{b+} k_{BA}^{a-}}{k_{BA}^{b-} k_{AB}^{a+}} \right) + \Gamma_{DC}^{b-} \ln \left(\frac{k_{DC}^{b-} k_{CD}^{a+}}{k_{CD}^{b+} k_{DC}^{a-}} \right) \right] \\ &= k_B \Gamma_O \ln \left(\frac{k_{AB}^{a+} k_{BD}^{r+} k_{DC}^{a-} k_{CA}^{r-}}{k_{BA}^{a-} k_{DB}^{r-} k_{CD}^{a+} k_{AC}^{r+}} \right) + k_B (\Gamma_{AB}^{b+} - \Gamma_{DC}^{b-}) \ln \left(\frac{k_{AB}^{b+} k_{BA}^{a-}}{k_{BA}^{b-} k_{AB}^{a+}} \right) + k_B \Gamma_{DC}^{b-} \ln \left(\frac{k_{DC}^{b-} k_{CD}^{a+} k_{AB}^{b+} k_{BA}^{a-}}{k_{BA}^{b-} k_{AB}^{a+} k_{CD}^{b+} k_{DC}^{a-}} \right) \\ &= \kappa \Gamma_O \left[\left(\frac{k_B}{\kappa} \right) \ln \left(\frac{k_{AB}^{a+} k_{BD}^{r+} k_{DC}^{a-} k_{CA}^{r-}}{k_{BA}^{a-} k_{DB}^{r-} k_{CD}^{a+} k_{AC}^{r+}} \right) \right] + \{\varepsilon_L \Gamma_{AB}^{b+} - (\varepsilon_L + \kappa) \Gamma_{DC}^{b-}\} \left[\left(\frac{k_B}{\kappa} \right) \ln \left(\frac{k_{BA}^{b-} k_{AB}^{a+} k_{CD}^{b+} k_{DC}^{a-}}{k_{DC}^{b-} k_{CD}^{a+} k_{AB}^{b+} k_{BA}^{a-}} \right) \right] \\ &\quad + (\Gamma_{AB}^{b+} - \Gamma_{DC}^{b-}) \left[k_B (1 + \theta) \ln \left(\frac{k_{AB}^{b+} k_{BA}^{a-}}{k_{BA}^{b-} k_{AB}^{a+}} \right) + k_B \theta \ln \left(\frac{k_{DC}^{b-} k_{CD}^{a+}}{k_{CD}^{b+} k_{DC}^{a-}} \right) \right]. \end{aligned} \quad (\text{E5})$$